In press, Interface Science LBNL-47270

Model Studies of Rayleigh Instabilities *via* Microdesigned Interfaces

Andreas M. Glaeser

Department of Materials Science and Engineering,
University of California,
&
Center for Advanced Materials
Lawrence Berkeley National Laboratory, Berkeley, CA 94720

Abstract

The energetic and kinetic properties of surfaces play a critical role in defining the microstructural changes that occur during sintering and high-temperature use of ceramics. Characterization of surface diffusion in ceramics is particularly difficult, and significant variations in reported values of surface diffusivities arise even in well-studied systems. Effects of impurities, surface energy anisotropy, and the onset of surface attachment limited kinetics (SALK) are believed to contribute to this variability. An overview of the use of Rayleigh instabilities as a means of characterizing surface diffusivities is presented. The development of models of morphological evolution that account for effects of surface energy anisotropy is reviewed, and the potential interplay between impurities and surface energy anisotropy is addressed. The status of experimental studies of Rayleigh instabilities in sapphire utilizing lithographically introduced pore channels of controlled geometry and crystallography is summarized. Results of model studies indicate that impurities can significantly influence both the spatial and temporal characteristics of Rayleigh instabilities; this is attributed at least in part to impurity effects on the surface energy anisotropy. Related model experiments indicate that the onset of SALK may also contribute significantly to apparent variations in surface diffusion coefficients.

Disclaimer

Copyright

Introduction

Polycrystalline ceramics are typically fabricated from powders with specific surface areas >1 m^2/g. Thus, the properties of the solid-vapor interfaces that dominate the initial microstructure, and of the grain boundaries that form at contact points between particles are important in defining the evolution of the microstructure. Scaling laws [1] indicate that the relative importance of surfaces and grain boundaries will only increase if particle sizes and grain sizes decrease further, *e.g.*, into the nanoscale regime.

The microstructural changes that occur during sintering as well as those that occur during high-temperature use are complex. The ultimate microstructure (density, grain size, grain size distribution) reflects the outcome of a competition between many concurrent processes. For sintering, it is convenient to view this as a competition between transport mechanisms that lead to densification (lattice and grain boundary diffusion) and those that promote coarsening (vapor transport and surface diffusion) as discussed by Yan [2] and by Brook [3]. As the particle and grain sizes are progressively reduced, the competition involving grain growth (coarsening) controlled by surface diffusion and densification controlled by grain boundary diffusion is likely to become increasingly pertinent. The rates will be proportional to the surface "thickness" (δ_s) surface diffusivity (D_s) product, and the grain boundary width (δ_b) grain boundary diffusivity (D_b) product, respectively. Analysis of this competition [2] indicates that a factor of 3-5 change in the $\delta_s D_s / \delta_b D_b$ ratio can result in substantial changes in the grain size-density trajectory. Thus, an understanding of how to modify the $\delta_s D_s / \delta_b D_b$ ratio would be of practical value.

More generally, from an experimental standpoint, theoretical models of specific densification-coarsening mechanism pairs provide opportunities for interpreting the effects of changes in temperature, sintering atmosphere, particle size, and impurity concentration on the path of microstructural evolution. Several studies have focussed on magnesia-doped aluminum oxide (see [4-6] and references therein), and more recently titania-doped aluminum oxide [7, 8] as model systems. Such analytical solutions also stimulate efforts to *independently measure* the $\delta_s D_s$ product, its dependence on temperature, and its sensitivity to dopant additions. Systematic studies of the effects of adding impurities spanning ranges of charge mismatch, size mismatch, solubility, etc., on $\delta_s D_s$ would be of great value.

The need for reliable transport data (and the difficulty of obtaining it) is not unique to ceramics. Numerous methods have been developed to identify the rate-controlling transport mechanism, and to extract the associated transport coefficient from measurements of morphological change. For ceramics, these include measurements of the neck growth rate in sphere-sphere and sphere-plate sintering experiments [9, 10], the growth rate of a grain boundary groove [11], and the decay rate of a periodic surface perturbation [12]. Measurements of the late stages of crack healing, a stage characterized by Rayleigh instabilities, have also been used in efforts to evaluate $\delta_s D_s$ [13-15]. Despite the obvious importance of surface diffusion, and many attempts to quantify $\delta_s D_s$, there is considerable scatter in the reported values. For example, in aluminum oxide, a well-studied model system, reported values of $\delta_s D_s$ at fixed elevated temperatures can span five or more orders of magnitude [14].

Impurities, either within the material or introduced inadvertently during experimentation, can alter the diffusion behavior. In extreme cases, a second phase may develop. The older surface diffusion literature for alumina shows a significant increase in surface transport rates when a calcium silicate second phase is present [16, 17]. Work by Baik and coworkers [18-21] has shown the extreme caution required to avoid inadvertent contamination. Segregation of impurities to surfaces can also be important, even if the impurity is present at low concentrations. Adsorbed impurities can affect the absolute and relative energies of surfaces, and thus alter the Wulff shape [22, 23], as demonstrated in experimental work by Choi *et al.* [24] and by Kitayama *et al.* [25-30] for alumina. Kitayama has shown that Ca^{2+}, Mg^{2+}, Ti^{3+}, and Ti^{4+} all affect the equilibrium shape of alumina in distinct ways. Of the common impurities in alumina, it is well known that calcium segregates to a number of surfaces in alumina, even when present at ppm levels. Sung *et al.* [31] have verified that magnesium segregates to pore surfaces. Several studies [32-35] have suggested that surface contaminants and segregated impurities such as calcium and silicon could be responsible for fundamental changes in the surface structure and properties of alumina, including the surface diffusivity. In addition, in systems in which facetting is prevalent, the development of facets can fundamentally change the rate-limiting step governing surface transport. As discussed in recent work by Mullins and colleagues [36-38], and suggested by the work of Kitayama *et al.* [27, 39, 40], nucleation of critical-size patches on facets

rather than diffusion may limit the rate of facet motion and cause large disparities in the *apparent* $\delta_s D_s$ values.

Collectively, the complications associated with impurities, surface energy anisotropy, and facetting-induced changes in transport mechanism impede the study and understanding of surface diffusion in ceramics. Our efforts have focussed on the development of methods of studying transport where surface contamination can be avoided, surface energy anisotropy effects are more clearly evident, and as a result, the effects of surface crystallography and doping can more easily be quantified [41-46]. Rayleigh instabilities provide a convenient means of studying surface transport, particularly in optically transparent ceramics. This paper reviews the progress made in applying Rayleigh instabilities to characterize surface transport in single crystal aluminum oxide (sapphire), a model ceramic material.

Background

Due to its widespread relevance to microstructural evolution, there have been many attempts to model the morphological stability of high aspect ratio phases in solids. The earliest modelling efforts focussed on breakup of fluid jets [47-49]. In solids, the morphological stability of fibers in a composite, rod-shaped phases in eutectic or eutectoid structures, pore channels in sintering materials, and of cracks at elevated temperature have important consequences for material properties and microstructural evolution, and are thus of interest to the materials community.

The spatial and temporal characteristics of Rayleigh instabilities have the potential to provide useful information relating to the energetic and kinetic properties of surfaces, respectively. This section attempts to review the evolution of our understanding of Rayleigh instabilities in solids.

Modelling History

As mentioned previously, the earliest modelling efforts focussed on the breakup of continuous fluid jets. The process of interest is schematically illustrated in Figure 1. At time t_0, a cylindrical body has only infinitesimal periodic perturbations. As time increases, perturbations of appropriate wavelength increase in amplitude. After sufficient time, the initially continuous phase evolves into a set of discrete droplets or

particles with some characteristic spacing. Plateau [47] and Rayleigh [48] accordingly considered a material with *isotropic* surface energy, γ_s, treated the jets as cylinders of radius *R*, and assessed the stability of such a cylinder to periodic perturbation of wavelength λ and (initially *infinitesimal*) amplitude α. Nichols and Mullins were the first to extend the method of Plateau and Rayleigh to solids, and evaluated the instability of solid cylindrical rods [50], as well as the breakup of cylindrical voids in a solid *via* surface or lattice diffusion [51]. For both cases, the amplitude at time *t* is related to the initial amplitude α_o by a growth/decay law of the form:

$$\alpha = \alpha_o \exp[\mu t] \tag{1}$$

The amplification factor μ is sensitive to the perturbation wavelength λ, and the specific form of the wavelength dependence is affected by the transport mechanism. For surface-diffusion-controlled evolution [51]

$$\mu = \frac{\delta_s D_s \gamma_s \Omega}{R^4 kT}\left[\left(\frac{2\pi R}{\lambda}\right)^2\left(1-\left(\frac{2\pi R}{\lambda}\right)^2\right)\right] = \frac{\delta_s D_s \gamma_s \Omega}{R^4 kT}\left[x^2\left(1-x^2\right)\right] \tag{2}$$

where Ω is the atomic volume, *R* the pore channel (or solid cylinder) radius, k*T* has its usual meaning, and *x* is the ratio $2\pi R/\lambda$. If $\lambda < 2\pi R$, then $\mu < 0$, and α decreases with time. It is apparent that $\mu \to 0$ when $\lambda \to 2\pi R = \lambda_{min}$ and when $\lambda \to \infty$, and as a result, evolution will be very sluggish when $\lambda \to \lambda_{min}$, and when λ is large. There is an intermediate value of λ for which the perturbation growth rate reaches its maximum value. For surface diffusion, this occurs when $x \approx 0.707$, or equivalently, when $\lambda = \lambda_{max} = \sqrt{2} \cdot \lambda_{min}$. If it is assumed that in a system with a spectrum of perturbation wavelengths, the infinitesimal perturbations with the maximum value of μ, *i.e.*, the highest growth rate, dominate the evolution, pores or particles spaced ≈8.89*R* apart should develop. If instead volume diffusion dominates, the predicted pore spacing is ≈12.96*R* [51]. Thus, in principle, the mechanism dominating perturbation growth can be determined from measurements of the pore size and spacing, or alternatively, from measurements of the pore spacing and knowledge of *R*. If α_o and the other materials and geometric parameters in the definitions

of μ are known, $\delta_s D_s$ or D_v (the volume self-diffusion coefficient) can be determined (or at least estimated).

These kinetic analyses generally assume that the perturbation amplitude is small, and are therefore strictly valid only for the initial stages of perturbation growth.† The effects of larger amplitude periodic perturbations on morphological evolution in isotropic systems have been considered by Sekerka and Marinis [54]. For a solid cylindrical rod of infinite length embedded in a matrix and evolving by interfacial diffusion their nonlinear analysis indicates that for infinitesimal initial perturbations, the kinetic maximum occurs when $\lambda = \lambda_{max} = \sqrt{2} \cdot \lambda_{min}$, as predicted by Nichols and Mullins [51]. However, as α_o increases, the kinetic maximum shifts to higher values of λ, specifically, $\lambda_{max} = \left[\sqrt{2} + 0.98 \cdot \left(\alpha_o / R\right)\right] \cdot \lambda_{min}$, and the time for pinchoff is also affected. For $\alpha_o = 0.1R$, the rates indicated by the nonlinear analysis exceed those predicted by the linear analysis by a factor of 2 when $\lambda / \lambda_{min} \approx \sqrt{2}$, and a factor of 5 when $\lambda / \lambda_{min} \approx 10$. A more recent non-linear analysis by Ma [55] has shown that a broader spectrum of evolution paths is possible when finite perturbations are present; a mapping procedure in terms of the dimensionless parameters $\lambda/2\pi R$ and α_o/R has been developed to prescribe the parameter space within which each distinct morphological path dominates.

The preceding analyses assume that a single perturbation wavelength dominates, and thus, a sharp spacing distribution is expected. In practice, pre-existing perturbations spanning a range of λ and α_o will be present. In view of the exponential growth law, Eqn. (1), a perturbation with a somewhat larger α_o, with a λ that differs by some amount $\Delta\lambda$ from the kinetic maximum λ_{max} may persist, and broaden the observed pore or particle spacing distribution. Choy *et al.* [56] have performed a nonlinear stability analysis of rods with a multiharmonic surface profile. When the initial perturbations are sufficiently small relative to *R*, the rods are predicted to break up with a spacing $\lambda \approx \lambda_{max} = \sqrt{2} \cdot \lambda_{min}$ and little scatter. As α_o increases, the observed average spacing will differ from $\sqrt{2} \cdot \lambda_{min}$, shifting to values that reflect the initial

† Since the perturbation amplitude increases exponentially with time, Rayleigh and others subsequently, have assumed that the wavelength that is initially dominant will dominate throughout breakup. An additional assumption is that the wavelength that has a maximum value of μ dominates quickly, and thus, that the final spacing of discrete pores or particles, λ, reflects λ_{max}. More recently, Hackney [52] and Ma [53] have questioned the validity of this last assumption as part of efforts to rationalize the substantial scatter in λ that is often experimentally observed.

spectrum of λ and α_o, and the scatter in the observed spacings will increase. For the wavelength distributions examined, the largest scatter in the spacing developed when α_o values were in the range 0.01*R* to 0.05*R*, *i.e.*, still relatively small in comparison to *R*. Thus, such small amplitude perturbations can shift the peak or mean of the spacing distribution, and can lead to an *apparent* λ_{max} that differs substantially from the "true" kinetic maximum indicated by a linear analysis. An analysis of experimental data for several systems has led Ma [53] to propose that for surface-diffusion-controlled evolution the observed spacings reflect the wavelength of the periodic perturbations *initially* present, *not* λ_{max}.[✠] Both of these cases, evolution dominated by a spacing $\lambda \approx \lambda_{max} = \sqrt{2} \cdot \lambda_{min}$ and evolution dominated by random natural perturbations, impose significant experimental limitations. Both situations preclude or impair efforts to systematically assess the effect of varying λ on the magnitude of μ.

The prior analyses all consider rods or cylinders of infinite length, and thus, do not take into account the perturbation produced in a finite-length rod by its ends. Nichols [57] considered such "end effects" in an analysis of the breakup of rod-shaped particles (pores) of finite length. A critical length-to-radius (L/R) ratio emerged below which a cylindrical rod or cavity would spheroidize and form a single particle or pore. For the isotropic surface energy systems considered, this critical L/R ratio, $(L/R)_{crit} = 14.4$. As L/R is progressively increased, first two, and then successively larger numbers of particles or pores are predicted to form. Nichols determined the aspect ratios at which transitions from two to three particles (pores) and three to four particles (pores) are expected.

In materials with anisotropic surface energy, λ_{min}, λ_{max}, and $(L/R)_{crit}$ are strongly influenced by the surface energy changes that arise as sinusoidal perturbations reorient the surface relative to the initial channel surface orientation. The evolution behavior is sensitive to the shape of the Wulff plot in the vicinity of the mean channel orientation. Thermodynamic and kinetic analyses of the morphological evolution of pore channels in anisotropic materials have been performed by Cahn [58] and by Stölken and Glaeser [59], respectively, to yield values of λ_{min} and λ_{max}, respectively. For the special case of transverse

[✠] These conclusions are based on comparing the experimentally measured values of pore or particle spacings to the values predicted for a material with *isotropic* surface energy. As will be discussed shortly, surface energy anisotropy can also introduce variability in the spacings.

isotropy, and surface-diffusion-controlled evolution, $\lambda_{max} = \sqrt{2} \cdot \lambda_{min}$ as in the isotropic case, however, λ_{min} depends upon the surface energy–surface orientation relationship. Specifically,

$$\lambda_{max} = \sqrt{2} \cdot 2\pi R\left(1 + \frac{1}{\gamma_s}\left(\frac{\partial^2 \gamma_s}{\partial \phi^2}\right)\right)^{\frac{1}{2}} = \sqrt{2} \cdot 2\pi R \cdot k_\gamma = \sqrt{2} \cdot \lambda_{min} \tag{3}$$

where γ_s is the surface energy at the mean channel orientation, $\phi = (\partial R/\partial z)$ where z is the axial coordinate, and thus $(\partial^2 \gamma_s / \partial \phi^2)$ is related to the curvature of the Wulff plot about the mean orientation. The observed pore spacing will increase or decrease from the value of $8.89R$ expected in an isotropic system, as dictated by the sign and magnitude of $(\partial^2 \gamma_s / \partial \phi^2)$. If the initial orientation corresponds to a sharp minimum in the γ_s-ϕ plot, $(\partial^2 \gamma_s / \partial \phi^2)$ will be large and positive, a substantial stabilization would be expected, and λ_{min} should exceed $2\pi R$. Conversely, when $(\partial^2 \gamma_s / \partial \phi^2) < 0$, λ_{min} will be $<2\pi R$.

Glaeser [60] has extended the analysis of Stölken and Glaeser [59] to quantify the effect of surface energy anisotropy on the *kinetics* of evolution for the same idealized anisotropic system. Both the value of λ_{max} (Eqn. (3)) and of μ are affected. For surface-diffusion-controlled evolution,

$$\mu = \frac{\delta_s D_s \gamma_s \Omega}{R^4 \mathrm{k} T}\left[x^2\left(1 - \left(1 + \frac{1}{\gamma_s}\left(\frac{\partial^2 \gamma_s}{\partial \phi^2}\right)\right)x^2\right)\right] \tag{4}$$

which reduces to Eqn. (2) for an isotropic system. It follows that if λ_{max} in an anisotropic system is k_γ times λ_{max} in an isotropic system, then for surface-diffusion-controlled evolution, the evolution time is $\left(k_\gamma\right)^2$ that in an isotropic system. Since values of $k_\gamma > 10$ have been observed [42, 44], anisotropy can cause significant changes in the evolution time. If evolution times are interpreted in the context of a model in which isotropic surface energy is assumed, such time changes can lead to significant changes and variations in the *apparent* surface diffusivity.

Experimental History

For liquids, experiments can be performed in which the system properties and the geometry closely match those that have been modelled. Cylindrical liquid jets can be emitted from a circular orifice. The jet

diameter can be controlled and varied. The surface tension is isotropic. As originally explored by Rayleigh, and more recently by others [61, 62], it is possible to use a disturbance, either sonic or mechanical, to produce a periodic perturbation of finite and controlled wavelength and amplitude on a liquid jet.

For solids, the situation is much more complex. High aspect ratio pore channels are produced in ceramics during crack healing, and as a result, crack healing experiments have provided the basis for studies of Rayleigh instabilities in ceramics. In conventional experiments, cracks are introduced using thermal shock or indentation. As a result, the crack geometry is not readily controlled. The pore channels that develop do not necessarily have a fixed "radius". Even in single crystals, the crystallographic orientation of the channels is not controlled, and often not known. The effects of surface energy anisotropy can vary from channel to channel. As a result, not only the spatial characteristics of evolution, but indeed the very morphological path can vary from crack to crack. In polycrystalline materials, intergranular cracks will sample an even wider range of surface orientation and anisotropy, and more varied evolution behavior can be expected [63].❖ Cross sections of pores are likely to be at least partially facetted, and for intergranular cracks the grain boundary that intersects the pore will distort the shape and modify the energy changes that accompany evolution. Significant stabilization can arise, depending upon the dihedral angle formed at the grain boundary-pore surface junction, and the number of grains bounding or coordinating the channel [65]. A more general discussion of crack healing in ceramics and the parallels between microstructural changes during crack healing and sintering can be found in reference [15].

Over the past 35 years, aluminum oxide in both polycrystalline form and single crystal (sapphire) form has been the subject of numerous studies of annealing-induced strength improvement/recovery due to crack healing [13-15, 63, 66-72]. Although several studies focussed exclusively on strength recovery, others addressed the morphological aspects of crack healing [13-15, 63, 70, 71]. Yen and Coble [13] assumed that the pore channels formed in sapphire during crack healing were cylindrical, isolated pores were spherical, and pore volume was conserved. The radii of selected pore channels were measured and compared with the spacing of pores after breakdown to determine the relationship between the dominant wavelength λ and R.

❖ For example, in systems with intergranular glassy films, flow of the glass may assist flaw healing. Such effects have been documented for ceramic/metal interfaces by De Graef *et al.* [64].

In addition, the radii of isolated pores and their spacings were measured. For surface-diffusion-controlled evolution, the expected spacing is $4.72\, r_p$, where r_p is the radius of an isolated pore, and for lattice-diffusion-controlled evolution the spacing is $6.07\, r_p$. Gupta [14] also inferred the dominant transport mechanism from the size and spacing of the isolated pores formed by Rayleigh instabilities during crack healing in polycrystalline alumina. Although considerable scatter in the calculated pore-spacing:pore-channel radius (λ/R) ratio was observed, both studies suggested that surface diffusion was the dominant transport mode. Maruyama and Komatsu [63] diffusion-bonded sapphire single crystals that were not perfectly planar and thereby produced controlled crack-face crystallography flaws at bicrystal interfaces. Their work showed that the grain boundary misorientation could affect the morphological evolution of intergranular flaws.

Experimental Approach

Experimentally, it would be desirable to produce and study the morphological evolution of channels with controlled geometry. The important geometric parameters are R and α_o. If R is precisely known, then it becomes possible to relate the measured pore spacings (assumed equal to λ_{max}) to R, and to quantify departures from isotropic behavior. For surface-diffusion-controlled evolution, the evolution time will scale as R^4 [1], and thus, if a determination of $\delta_s D_s$ is to be attempted, precise control over R is obviously critical. In a crystalline system, the stabilization due to surface energy anisotropy effects will depend upon the surface crystallography, and thus, it is desirable to control the crystallographic orientation of pore channels as well. If one can define and vary the channel (or rod) orientation one can quantify this stabilization effect. If the materials parameters such as γ_s and Ω are known, and the temperature T is controlled, one can in principle calculate the $\delta_s D_s$ product. Finally, if both the geometry and orientation can be controlled and reproduced in materials of known and systematically varied impurity content, then the effects of impurity additions on surface energy anisotropy can be isolated and assessed more easily.

The combination of photolithography and ion beam etching when applied to single crystals of known orientation allows the development of shallow, controlled-geometry cavities in the substrate surface.

Detailed descriptions of the techniques and processing parameters have been published previously [73], and as a result, only a brief summary is provided here. An advantage of lithography is the ability use mask design software to define the two-dimensional shape that is developed on the surface, and to "print" this pattern multiple times on the same substrate surface. Simple geometric shapes such as squares and rectangles and "lines" of controlled length and width (L/D ratio) are easily produced. As will be shown, more complicated shapes including pore channels with a predefined λ and α_o can also be produced. A significant advantage of the lithographic method is that depending upon the feature size and the size of the substrate, literally tens of thousands of features can be generated in a single sample. Features with different geometry or different size or both can be produced in the same specimen. These features have a characteristic width (parallel to the surface) of ≥2 μm, and a depth that is characteristically on the order of 0.1-0.5 μm. The processing of the surfaces is performed under Class 100 clean-room conditions, and thus, cleanliness of the surfaces can more readily be maintained.

The transfer of these features to an internal interface is achieved by solid-state diffusion bonding of the etched substrate to an unetched substrate. If both substrates are single crystals, the orientations are appropriately matched, and the substrates are carefully aligned, then at worst a low angle twist boundary (<2°) develops along the bond plane. Consequently, after bonding, the surface cavities approximate intragranular cavities. It is also possible to intentionally misorient the two crystals and simulate intergranular defects. Other options for the character of the interface produced by bonding have been described in reference [73]. For the Rayleigh instability studies, the primary emphasis has been on developing either semi-infinite or controlled aspect ratio (L/D) pore channels with their axes aligned along specific directions within the basal (0001) plane of sapphire. Most often [42-44, 46], orthogonal sets of pore channels were introduced, with axes aligned parallel to $[1\bar{1}00]$ and $[11\bar{2}0]$. In some cases [43, 44], the chemistry of the sapphire surface was modified by ion implantation. The original channel geometry and the channel orientations could then be duplicated to isolate the effects of impurities on the evolution. Pore channels have also been progressively rotated by controlled angular increments to allow a more thorough assessment of orientation effects on stability [46]. Finally, it is possible to design a feature pattern such that a finite perturbation of controlled amplitude and wavelength is introduced [45]. This facilitates systematic

study of the dependence of the amplification factor μ on λ. For more detailed accounts of the materials characteristics, sample preparation and other experimental procedures the interested reader is referred to the cited references.

Several additional advantageous features and characteristics of this experimental approach should be emphasized. Since the pore channels are internal, the surfaces are isolated from the furnace environment, and thus, the likelihood of inadvertent surface contamination is reduced. For opaque materials, evaluation of the extent of evolution is difficult, and the sample must be destroyed in order to obtain the necessary morphological information. In contrast, for optically transparent ceramics such as sapphire, the evolution can be monitored nondestructively, and it is this feature, as well as the availability of single crystals of controlled surface orientation that made this approach particularly attractive.

Results and Discussion

Semi-Infinite Pore Channels

Effects of channel orientation

Rödel [42] performed the first study of Rayleigh instabilities utilizing this microfabrication approach. Semi-infinite pore channels were etched into the (0001) and $(11\bar{2}0)$ planes of *undoped* sapphire. At 1800°C, channels oriented parallel to the $[1\bar{1}00]$ and $[11\bar{2}0]$ directions of the (0001) plane developed periodic perturbations whose amplitude increased with time, and ultimately led to the breakup of the pore channels into a series of isolated pores. Optical micrographs of pore channels illustrating the initial geometry and the subsequent stages of evolution are shown in Figure 2. The measured pore spacings (λ) were related to the equivalent circular radius of the pore channel, hereafter referred to as *R*.[✡] Channels oriented parallel to the $[1\bar{1}00]$ and $[11\bar{2}0]$ directions evolved into pores with mean spacings of 30.2-37.4*R* and >200*R*, respectively. Both values are well above that expected for an isotropic material (8.89*R*), and differ substantially from each other.

[✡] The as-etched pore channels have a rectangular cross section. *R* represents the radius of a cylinder that has the same cross-sectional area. Since *R* typically varies from sample to sample, it is convenient to express pore spacings as multiples of *R* or to normalize the spacing by *R* and quote and compare (λ/R) values.

Powers [44] subsequently performed similar pore channel evolution experiments on (0001) undoped sapphire; in this case, samples were annealed at 1700°C. The method of sample assembly differed from that used by Rödel [42] and introduced a twin boundary. In these experiments, pore channels oriented along the $[1\bar{1}00]$ and $[11\bar{2}0]$ directions of the etched crystal broke up with characteristic mean spacings of ≈45*R* and 130*R*, respectively. Although the *relative* stability trend for channels oriented parallel to the $[1\bar{1}00]$ and $[11\bar{2}0]$ directions was duplicated, the mean values differed from those reported by Rödel.

In recent work [46], semi-infinite channels of L/R ratio of ≈1250 and ≈1020 were produced in (0001) undoped sapphire. The channel axis was rotated in 15° increments to produce individual arrays containing 24 channels, as shown in Figure 3a. The pattern was aligned so that selected channels within the set were parallel to the $[1\bar{1}00]$ and $[11\bar{2}0]$ directions of the etched crystal. One sample was prepared with a twin boundary, the other duplicated the assembly method described by Rödel, which produces a very low angle basal twist boundary. In the sample with the twin, the prior results of Powers [44] were duplicated. For the sample without the twin, the *relative* stability was consistent with the earlier results of Rödel [42], but mean λ values of ≈70*R* and ≈195*R* were obtained for the $[1\bar{1}00]$- and $[11\bar{2}0]$-oriented channels.

In all cases, the scatter in the λ values was significant, with the standard deviation ≈30% of the mean value. This suggests that the ultimate pore spacings are affected by inherent or natural perturbations present at the initial stages of evolution. However, the inherent or natural perturbations in the channel cross section that would form during processing of the defect patterns would be expected to be independent of the orientation of the substrate surface, and also of the direction within the substrate plane. (Samples are rotated continuously during ion beam etching.) Thus, the observations suggest that the observed directional variation is (at least in part) due to a stabilization effect resulting from surface energy anisotropy that varies as the orientation of the channel varies within the basal plane.

When evolution patterns in the 24-channel arrays illustrated in Figure 3a were quantified, there was indeed a systematic variation in mean λ/R values as the channel orientation changed. λ/R values exhibited a minimum for the $[1\bar{1}00]$-oriented channels, and increased as the $[11\bar{2}0]$ direction was approached. The observed variation did not exhibit the symmetry expected for channels aligned parallel to

(0001). As discussed in reference [46], we believe that this reflects the effect of a miscut of the crystal, and thus, a deviation of the surface from its ideal orientation. Indeed, small and uncontrolled variations of the miscut together with small random alignment differences may contribute to the sample-to-sample differences in mean λ/R values among samples with channels of *nominally* the same orientation. The beautiful work of Surnev *et al.* [74] provides a very clear demonstration of miscut effects and perturbation alignment on surface morphology evolution during the smoothing of a periodic perturbation on gold (111) vicinal surfaces.

Effect of impurities

Efforts to characterize the effects of impurities on the spatial characteristics of channel breakup exploited substrates in which the surface composition was modified by ion implantation [43, 44]. The impurity concentrations were maintained at low levels to minimize the potential for implantation damage, and multiple implantation runs were performed with different implantation energies in an effort to flatten the compositional profile. Using this approach, sapphire substrates with near-surface layers enriched in magnesium, calcium, and titanium were produced. Channels were etched into an implanted surface, and two similarly implanted substrate surfaces were bonded to produce internal pore channels.

Results of experiments in which channels of similarly high aspect ratio and (nominally) identical orientation were examined showed that each of the impurities had a distinct effect on the evolution behavior. Magnesium, generally thought to homogenize the surface properties of alumina, yielded mean λ/R values somewhat closer to those expected in an isotropic system, and reduced the difference in the characteristics of $[1\bar{1}00]$- and $[11\bar{2}0]$-oriented channels. Titanium implantation *reversed* the relative stability of the $[1\bar{1}00]$- and $[11\bar{2}0]$-oriented channels; channels oriented parallel to $[1\bar{1}00]$ appeared to be completely resistant to breakup. For calcium-implanted material, only channels oriented parallel to $[11\bar{2}0]$ etched well, and thus only their evolution was studied. However, for this orientation, three sets of channel with equivalent circular radii of 0.32, 0.50 and 0.71 μm were prepared by varying the channel width. The measured pore spacings were taken to be a measure of the kinetically dominant wavelength, and were normalized by the respective values of R. The statistics are summarized in Table I, and a comparison of the pore spacing distributions is provided in Figure 4. The mean λ/R ratios range from 61.7 to 64.6, and

are thus significantly greater than that expected in an isotropic material. Note that the normalized break-up characteristics are *virtually identical*. Similar constancy of mean λ/R ratios was evident in titanium-implanted sapphire as well when channels with equivalent circular radii of 0.29 and 0.44 μm were compared [44]. Such behavior would not be expected if evolution were solely dominated by inherent perturbations. Perturbations with a fixed range of λ interacting with channels of differing R would have produced shifts in the λ/R distributions.

Preperturbed Pore Channels

As was observed in the case of fluids, model experiments in which the perturbation wavelength and amplitude can be controlled and systematically varied provide a means of increasing our knowledge of the breakup process, and can bring new evolution paths to light. In prior studies of morphological instabilities of rodlike particles and pore channels in solids, relatively wide particle or pore spacing distributions were observed. It was thus desirable to develop experimental procedures that would allow more precise control over the geometry of high aspect ratio internal phases within solids. Achieving this was more difficult than for liquids.

Effects of channel orientation

In lithographic processing, a mask is designed so that a specific pattern of geometric features (holes) is produced in the photoresist on the substrate surface. During subsequent ion beam etching, the substrate is selectively etched where there are holes in the resist, and thus, the mask pattern is transferred to the substrate. Kulinsky *et al.* [45] generated masks containing semi-infinite channels with sinusoidal perturbations of controlled wavelength and fixed amplitude. The imposed perturbation wavelength, λ_{imp}, was varied by a factor of 10, with values ranging from 25 μm to 250 μm. These variations are imposed on the channel *width*; the channel depth is initially constant, and controlled by the etching parameters. As in prior studies, (0001) sapphire wafers were used, and the channel axes were aligned parallel to $[1\bar{1}00]$ and $[11\bar{2}0]$. Post-bonding anneals were conducted at 1650°C.

Due to the relatively low temperatures used during bonding, *e.g.*, 1300-1400°C, little if any morphological change occurs during the internalization of the pore channels. Thus, after diffusion bonding,

the pore channels are much wider than they are deep. An example of the initial pore channel morphology is shown in Figure 5a. When subsequent anneals are performed at higher temperatures, *e.g.*, 1650°C, mass transport produces more significant shape changes. For most perturbation wavelengths, mass transport in the plane normal to the channel axis occurs over distances that are short in comparison to λ_{imp}, and the cross-sectional shapes deviate substantially from the equilibrium shape. As a result, the development of a more equiaxed cross section generally precedes axial instability, Figure 5b, and results in channels with controlled wavelength axial perturbations, more closely resembling those illustrated in Figure 1b.

The factor of 10 variation in λ_{imp} yields a factor of 10 variation in λ_{imp} / R. The etching conditions were such that in many cases the perturbations spanned a sufficiently broad range of λ_{imp} that the shortest wavelengths were less than λ_{min}, and the longer wavelengths were much greater than λ_{max}. This provided a number of unique experimental opportunities. By monitoring the transition from amplitude decay to amplitude growth, it was possible to experimentally determine λ_{min}. By selecting the perturbation amplitude to be on the order of 0.1*R*, several distinct perturbations with $\lambda > \lambda_{min}$ had a sufficient growth rate advantage that the final pore spacing was narrowly bounded and equal to λ_{imp}. An example of this behavior is shown in Figure 5c for channels with wavelengths in the 100-250 μm range. By monitoring the evolution time within this intermediate wavelength range, it became possible to explore the relationship between λ and μ for the first time. When λ_{imp} is sufficiently greater than λ_{max}, breakup is slow, and the ligaments that form can be off sufficient length to undergo a further breakup into two or more pores. If this occurs, it will lead to values of λ that are less than λ_{imp}. Thus, provided that λ_{imp} spans a sufficiently wide range, all three indicated evolution patterns should be observed in an experiment. For many of the experimental conditions examined previously, and those currently under study, two or more of these patterns were observed.

For all samples investigated, the smallest values of λ_{imp} appeared to lie in the range where $\lambda_{imp} < \lambda_{min}$. As a result, the imposed perturbations decayed with time and were replaced with longer wavelength perturbations that arose "naturally". For all samples investigated, this transition occurred at values of λ_{imp} that were well above those expected in an isotropic system. In samples where pore channels were oriented parallel to both the $[1\bar{1}00]$ and $[11\bar{2}0]$, the relative values of λ_{min} were consistent with the

relative stability trends indicated in prior work on semi-infinite pore channels. The ultimate pore spacing distributions were relatively wide, especially in comparison to samples where λ was dictated by λ_{imp}.

When $\lambda_{imp} > \lambda_{min}$ but does not exceed λ_{max} by too large an amount, one breakup event occurs per imposed wavelength. Figure 5c shows a region in which even the longest wavelength perturbations ($\lambda_{imp} = 250\ \mu m$) resulted in an initial breakup with $\lambda = \lambda_{imp}$. It appears that further annealing could potentially lead to the formation of two particles per elongated pore ligament. Figure 5d shows a different region along the same set of channels to indicate that breakup is occurring along the entire length of the pore channel, and is not complete everywhere. In addition, there are occasional variations in the spacing along the length.

In some cases, the anneal time increments were sufficiently small that it was possible to identify or at least bracket the wavelength range within which the most rapid evolution occurred, and to provide an estimate of the breakup time as a function of λ_{imp}. Such measurements indicate that when $[1\bar{1}00]$- and $[11\bar{2}0]$-oriented channels are compared, significant differences in λ_{max} and the associated minimum evolution time (t_{min}) can exist. However, an analysis of Eqn. (4) indicates that when evolution times (t) are scaled by the evolution time for the most rapidly evolving channels (t_{min}) and λ_{imp} is normalized by λ_{max}, the data, when replotted in terms of these normalized variables should fall on a single master curve given by

$$\frac{t_{min}}{t} = \frac{\mu}{\mu_{max}} = \left[\left(\frac{\lambda_{max}}{\lambda}\right)^2 \left\{2 - \left(\frac{\lambda_{max}}{\lambda}\right)^2\right\}\right] \qquad (5)$$

This normalization was successful in reducing the significant disparities that were apparent in evolution times and wavelengths [45], and thus appears to provide a useful albeit oversimplified framework for taking into account the effects of surface energy anisotropy.

For samples in which the larger values of λ_{imp} exceed λ_{max} sufficiently (see Figures 5c and 5d), there is the possibility of further breakup of the ligaments formed, or alternatively, the emergence of perturbations with a wavelength that reflects λ_{max}. In the latter case, an increase in the width of the pore or particle spacing may arise. Our study of this wavelength regime is incomplete.

Effect of impurities

In principle, systematic studies of the effects of specific impurity additions on λ_{min}, λ_{max}, and t_{min} should be possible. However, implantation affects only the near-surface region, and the resolution limits of conventional lithography required that the initial widths and therefore the ultimate channel radii be significantly larger than for nominally unperturbed channels. Due to the relatively larger pore radius, typically >1.5 μm versus <0.5 μm, the pore surfaces would extend beyond the implanted region after cross-sectional equilibration. As a result, studies to date have focussed on commercially available, melt-grown sapphire crystals that are expected to have a spatially uniform titanium doping level. Since (0001) substrates are not available, they were prepared by cutting slices from the top "shoulder" region of a titanium-doped single crystal boule. Laue measurements suggest that the miscut for these wafers was larger (≈3°) than those of commercially prepared wafers, which is more typically <2°.

Channels oriented parallel to $[11\bar{2}0]$ evolved in a manner qualitatively similar to that shown in Figure 5. As in the undoped samples, the apparent value of λ_{max} was less than that suggested by the mean pore spacing for channels in titanium-implanted samples that were initially unperturbed (as shown in Figure 2a). It is possible that as channels aligned along low-index directions, for which the channel perimeter is likely to contain facets, are perturbed artificially, the resistance to further perturbation growth offered by surface energy anisotropy is reduced.[⌘] Possibly related evidence is provided by the behavior of channels oriented parallel to $[1\bar{1}00]$, which are highly stable when unperturbed, followed a previously unobserved path of evolution when perturbed. As shown in Figure 6, rather than first equilibrating the cross-section, the perturbed edges apparently became unstable, developed instabilities and ultimately islands of pores with spacings unrelated to λ_{imp}. Such pathological behavior may arise because the etched in pattern perturbs the edge from its "stable" orientation, and moves the surface normal out of the cusp. Further work examining the evolution of $[1\bar{1}00]$-oriented channels is in progress, in an effort to determine

[⌘] Experiments in which the amplitude of the perturbation is progressively decreased might be useful in assessing this possibility. Alternatively, or additionally, the systematic rotation of the preperturbed channels could be useful in determining whether the reduction is largest for channel orientations where bounding facets can extend along the length of the cylinder. To eliminate miscut differences, both unperturbed and perturbed channels could be introduced into the same sample, allowing a more direct and meaningful comparison.

whether the surface modulation or the larger than normal miscut or both combined to produce such an evolution path.

Finite aspect ratio Pore Channels

Early work using microlithography to examine the break-up of controlled aspect ratio pore channels focussed on studies of the (0001) in undoped sapphire, and monitored the evolution of channels with aspect ratios varying from ≈10 to ≈156 at 1800°C [42]. For $[1\bar{1}00]$-oriented channels, those with L/R < 94 evolved into a single pore, only 5% of the channels with L/R = 94 evolved into multiple pores, and only ≈15% of the pores with the highest aspect ratio examined (L/R = 156) evolved into multiple pores. Channels oriented parallel to the relatively more stable $[11\bar{2}0]$ spheroidized. These observations indicate that $(L/R)_{crit}$ exceeds the value of 14.4 expected in an isotropic material, and thus, parallels the behavior seen for λ_{min} and λ_{max}.

In a more detailed study of finite aspect ratio pore channels a wider range of aspect ratio was examined, and channel orientation effects were more thoroughly probed [46]. Break-up of the varying aspect ratio channels, illustrated in Figure 3b, depended upon channel orientation, and followed a pattern what was similar to that observed for semi-infinite channels, as illustrated for undoped sapphire in Figure 7. Transitions from spheroidization to ovulation can be seen within the arrays at positions (L/R) values that vary with orientation. Both the energetics and the kinetics are affected. The critical aspect ratio, $(L/R)_{crit}$, varied from a low of ≈120 for channels oriented near to $[1\bar{1}00]$ to an unspecified value >250 for channels oriented parallel to $[11\bar{2}0]$; for the $[11\bar{2}0]$-oriented channels, even the highest (L/R) features in the array spheroidized. The average values of $(L/R)_{crit}$ range from ≈8× to ≈18× the value predicted by Nichols for an isotropic material. As with the semi-infinite pore channels examined in this study, the transition between the minimum and maximum breakup spacings was relatively smooth, with few small discontinuities.

In isotropic systems with surface-diffusion-controlled evolution, $(L/R)_{crit}$ lies between $2\cdot\lambda_{min}/R$ (≈12.6), and $2\cdot\lambda_{max}/R$ (≈17.8), and the ratio of $(L/R)_{crit}$ to (λ_{max}/R) is ≈1.62. For the semi-infinite channels, (λ/R) varied by a factor of ≈3, and $(L/R)_{crit}$ varied by a factor of ≥2.3 as the channel orientation is varied. Excluding the data for $[11\bar{2}0]$-oriented channels, for which $(L/R)_{crit}$ could not be determined, the

ratio $(L/R)_{crit}/(\lambda/R)$ varies between ≈2.3 and ≈3.1, with an average value of ≈2.7. Thus, the ratio is somewhat higher than that in an isotropic system.

Concluding Remarks

The treatment of Rayleigh instabilities has been and continues to be a topic of great interest. Considerable progress has been made in modelling the stability of high aspect ratio phases in solids, and high aspect ratio solid phases. Experimental capabilities have been expanded, and some important variables that affect the morphological evolution of elongated cavities, and by extension, elongated condensed phases have been examined. The following is an attempt to both summarize this paper and to provide some thoughts on areas where further experimental refinement is needed, and where the sophistication of the modelling needs to be increased.

Studies of the morphological evolution of lithographically introduced cavities in sapphire show that that both the spatial and temporal characteristics of evolution depend upon the crystallographic orientation of the channel. More recently, work on silicon carbide single crystals [75] indicates a similar trend. The deviation of the mean pore spacing from that expected in an idealized isotropic solid is believed to reflect the influence of surface energy anisotropy. In some cases, this influence manifests itself in an obvious way, by the development of well-defined facets [75], while in other cases, facets, if they are formed, are not obvious, but the deviations from isotropic behavior are nonetheless pronounced.

When the morphological evolution of large arrays of nominally identical features is tracked, features of identical geometry and orientation within the same specimen tend to show similar evolution patterns and rates. However, significant differences arise when cavities of nominally identical geometry and orientation introduced in *different* samples are compared. This is evident in the summary of data for pore channels in undoped sapphire provided in Table II. It is noted that although λ_{max} always exceeds the value expected in an isotropic material, and λ_{max} for $[11\bar{2}0]$-oriented channels always exceeds that for $[1\bar{1}00]$-oriented channels in the same sample, the mean values for a given orientation can vary by a factor of two or more. When the behavior of unperturbed and preperturbed semi-infinite channels of identical orientation

are compared, differences of up to a factor of four in λ_{max} are evident. Preliminary indications from on-going work involving preperturbed pore channels suggest that although the behavior from similar features within a given sample is generally consistent, sample-to-sample variations in λ_{max} are again apparent. Thus, experimentally, there are variables that are not yet adequately controlled.

One plausible explanation of these behavioral differences is that they are the result of small but random substrate-to-substrate variations in the miscut, coupled with small but random errors in aligning the pattern with the intended crystallographic direction. These variations would be expected to influence the stabilization effect arising from surface energy anisotropy.[⌘] The introduction of a finite amplitude perturbation would also reorient the surface. If this reorientation takes the surface normal out of a local surface energy minimum, this could help rationalize the observed *reduction* in λ_{max} relative to that characterizing breakup of an initially unperturbed channel. The direction of the shift is *opposite* of that predicted for an isotropic material [54].

A comparison of the evolution behavior of pore channels having similar orientation in doped versus undoped sapphire suggests that impurities modify the spatial characteristics of evolution. One can envision scenarios where a change in surface energy anisotropy, if not accounted for, could lead to entirely incorrect conclusions regarding the effect of the impurity on $\delta_s D_s$, a topic discussed in reference [60]. Recent work [25] has shown that the impurities that were implanted also change the equilibrium shape of alumina, and thus, changes in the energetics of surfaces and the associated surface energy anisotropy are not surprising. Fortunately, the samples that were studied came from a single set of sapphire crystals that are expected to have the same miscut. In future work assessing impurity effects it would be desirable to prepare specimens in which this constancy of the miscut is assured. The use of ion implantation to produce doped surfaces is convenient, but also imposes several experimental limitations. Although samples are preannealed to remove or minimize the implantation damage, the implanted layer is shallow, and depletion of the impurity during prolonged high-temperature anneals is a concern. The development of thicker and more uniformly doped

[⌘] Bonzel and co-workers have treated the effects of surface energy anisotropy on the *decay* of a periodic surface perturbation [76-78]. Their results indicate that the manner in which the surface energy varies with the orientation of the surface normal, i.e., the shape of the minimum in surface energy-surface orientation plot, can have an important impact on profile shape adjustments and decay rates. Such effects should also be important during perturbation *growth*.

surface layers by the epitaxial growth of an oriented single crystal seed through a doped polycrystalline layer [79] provides an attractive alternative to previously used methods.

Although the spatial characteristics of Rayleigh instabilities may very well depend sensitively on the specific miscut of the crystal, the use of preperturbed pore channels may nonetheless provide a convenient method of assessing the surface diffusivity. The original work of Kulinsky *et al.* [45] implied values of $\delta_s D_s$ that were on the high end of the substantial range indicated in prior studies, and suggested that titanium doping increased the surface diffusivity. Recent work has focussed on reexamining the evolution of preperturbed pore channels in a larger number of specimens that are likely to span a broader range of miscut and misalignment. In such experiments, one generally identifies a range of λ within which λ_{max} lies, and a range of time within which t_{min} lies. Despite these uncertainties in the exact value of λ_{max} and t_{min}, and variations in λ_{max} and t_{min} from sample to sample, the linear analysis suggests that $\delta_s D_s$ varies by at worst a factor of ≈7 from sample to sample, and the range of values is consistent with values deduced in the previous work. Although the use of a linear analysis is a concern, the results are of value in at least a comparative sense, and the sample-to-sample agreement in $\delta_s D_s$, despite significant differences in λ_{max} and t_{min}, is encouraging.

Collectively, the results imply that experimental studies of Rayleigh instabilities will need to be more attentive to controlling and characterizing the miscut. Extensions of experiments like those described by Surnev *et al.* [74] on the smoothing of periodic surface perturbations may be required. The fabrication, etching, and subsequent diffusion bonding of substrates with controlled miscut will add further complexity to an already challenging experimental procedure. However, when such experiments are performed on materials with known miscut and with spatially uniform impurity contents, the effects of interest should be more reproducible and more amenable to analysis.

With respect to modelling, it would be desirable to refine the existing models so that they more accurately treat the geometry in anisotropic materials, and take into account the effects of larger amplitude perturbations on the energetics and kinetics of evolution. Initial efforts to include the effects of facetted cross sections on the energetics of evolution have focussed on channels that facet to form regular polygons in the cross section. For such facetted channels, the energy changes associated with perturbation growth,

and the resulting value of λ_{min} are most simply related to the radius of the circle that *circumscribes* the polygon, R_{circ} [80]. In contrast, the comparisons made between theoretical predictions and experimental data have generally utilized the radius, R, of the circle that has an equivalent cross-sectional area. Although the use of R rather than R_{circ} when evaluating facetted rods or cavities introduces errors, the errors that result appear to be relatively small. Thus, the dominant contribution to deviations from the predictions for λ_{min} (and λ_{max}) in isotropic materials will again be expected to come from the surface energy anisotropy. Nonlinear treatments of the capillary instability of high aspect ratio features with isotropic surface energy have been developed; analogous treatments for anisotropic materials have not. As a result, diffusivity values that are extracted from experimental studies should be treated with appropriate caution, since the errors could be significant.

An important concern in extracting transport coefficients from the evolution behavior of facetted channels is the extent to which the evolution hinges not on surface diffusion, but is instead limited by other processes. In a recently published study of pore shape relaxation rates in sapphire, Kitayama *et al.* [27] found that when pores of nonequilibrium shape were bounded by stable facets, the evolution rates can be much lower than expected. If interpreted in terms of surface-diffusion-limited-evolution, the rates led to values of $\delta_s D_s$ that were lower than expected and decreased with time. In contrast, when the cavities were bounded by unstable surfaces that should rapidly evolve into fine-scale hill-and-valley structures, the evolution rates were much higher and the implied $\delta_s D_s$ values were within the range expected for surface diffusion control. These observations, more fully discussed in reference [27], suggest that an attachment/detachment process, or the nucleation of critical size patches of atoms or holes in facets may limit the rate of facet advance or retreat. The recent work of Mullins and Rohrer [38] addresses this latter issue. When dislocations fail to provide an adequate density of ledges at which atom attachment or detachment can occur, the movement of a facet normal to itself can be limited by a nucleation event. Similar considerations should apply during Rayleigh instabilities, and such nucleation barriers may be involved in kinetically stabilizing (unperturbed) $[1\bar{1}00]$-oriented channels in titanium-implanted sapphire [44]. The comparatively rapid breakup of similarly oriented pore channels that were preperturbed may reflect a lowering of the energy barrier due to surface energy anisotropy, but could also be due to the perturbation

providing additional attachment/detachment sites. Studies using atomic force microscopy of stable and partially broken up channels might be useful in addressing this issue.

Finally, this paper has focussed almost exclusively on experimental results obtained in a single material, alumina, and in large part on results obtained using single crystal sapphire substrates. Moreover, the focus is on the evolution of cavities within these materials. The spectrum of problems where Rayleigh instabilities are important is certainly broader, and includes problems where it is a solid phase that undergoes the instability, and also where a thin liquid film sandwiched between solids undergoes similar morphological changes. In these cases, the crystallographic character of the bounding surfaces is also likely to be important and may have contributed to departures from the behavior expected in isotropic systems, and resulted in "scatter" in the measurements. In principle, the lithographic tools that have been developed, when coupled with deposition techniques, may provide a means of studying these evolution processes under more controlled circumstances as well.

Acknowledgements

J. W. Rödel, J. D. Powers, J. S. Stölken, L. Kulinsky, and M. Kitayama performed the research described in this paper, and their contributions are gratefully acknowledged. Research support for the work in references [6, 27, 40-42] was solely provided by the Director, the Office of Energy Research, Office of Basic Energy Sciences, Materials Sciences Division of the U.S. Department of Energy under Contract No. DE-AC03-76SF00098. The work in references [28-30, 43-46] was supported by the National Science Foundation under a series of grants, most recently, Grant No. DMR-9617392. The work described would not have been possible without the assistance of the technical staff of the Microfabrication Laboratory in the Department of Electrical Engineering and Computer Science at the University of California at Berkeley. I have benefitted greatly from numerous discussions with too many colleagues to list individually. Discussions with Rowland Cannon over a period of many years have been particularly stimulating and beneficial. Finally, this manuscript was prepared while on a sabbatical leave at the Eindhoven University of Technology in The Netherlands. The hospitality of the faculty, staff and students was greatly appreciated.

References

1. C. Herring, "Effect of Change of Scale on Sintering Phenomena," *J. Appl. Phys.*, **21**, [4], 301-03 (1950).
2. M. F. Yan, "Microstructural control in the processing of electronic ceramics," *Mater. Sci. Eng.*, **48**, [1], 53-72 (1981).
3. R. J. Brook, "Fabrication Principles for the Production of Ceramics with Superior Mechanical Properties," *Proc. Brit. Ceram. Soc.*, **32**, [1], 7-24 (1982).
4. K. A. Berry and M. P. Harmer, "Effect of MgO solute on microstructure development in Al_2O_3," *J. Am. Ceram. Soc.*, **69**, [2], 143-9 (1986).
5. S. J. Bennison and M. P. Harmer, "Effect of Magnesia Solute on Surface Diffusion in Sapphire and the Role of Magnesia in the Sintering of Alumina," *J. Am. Ceram. Soc.*, **73**, [4], 833-37 (1990).
6. J. Rödel and A. M. Glaeser, "Pore Drag and Pore-Boundary Separation in Alumina," *J. Am. Ceram. Soc.*, **73**, [11], 3302-12 (1990).
7. J. D. Powers and A. M. Glaeser, "Titanium Effects on Sintering and Grain Boundary Mobility of Alumina," *Ceram. Eng. Sci. Proc.*, **18**, [4], 617-23 (1997).
8. J. D. Powers, "Titanium Effects on Microstructure Development in Alumina," Ph. D. thesis, Department of Materials Science and Mineral Engineering, University of California, Berkeley, (1997).
9. G. C. Kuczynski, "Self-Diffusion in Sintering of Metallic Particles," *Trans. A. I. M. E.*, **185**, [2], 169-78 (1949).
10. R. L. Coble, "Initial Sintering of Hematite and Alumina," *J. Am. Ceram. Soc.*, **41**, [2], 55-62 (1958).
11. W. W. Mullins, "Theory of Thermal Grooving," *J. Appl. Phys.*, **28**, [3], 333-39 (1957).
12. W. W. Mullins, "Flattening of a Nearly Plane Solid Surface due to Capillarity," *J. Appl. Phys.*, **30**, [1], 77-83 (1959).
13. C. F. Yen and R. L. Coble, "Spheroidization of Tubular Voids in α-Al_2O_3 Crystals at High Temperatures," *J. Am. Ceram. Soc.*, **55**, [10], 507-9 (1972).
14. T. K. Gupta, "Instability of cylindrical voids in alumina," *J. Am. Ceram. Soc.*, **61**, [5-6], 191-5 (1978).
15. T. K. Gupta, "Crack Healing in Al_2O_3, MgO, and Related Materials," in Advances in Ceramics, vol. 10, W. D. Kingery, Ed. Columbus: The American Ceramic Society, 1984, pp. 750-66.
16. W. M. Robertson and F. E. Ekstrom, "Impurity Effects in Surface Diffusion on Aluminum Oxide," in The Role of Grain Boundaries and Surfaces in Ceramics, vol. 3, *Materials Science Research*, W. W. Kreigel and H. Palmour, Eds. New York: Plenum Press, 1966, pp. 273-283.
17. J. M. Dynys, R. L. Coble, W. S. Coblenz, and R. M. Cannon, "Mechanisms of Atom Transport during Initial Stage Sintering of Al_2O_3," in Sintering Processes, G. C. Kuczynski, Ed. New York: Plenum Press, 1980, pp. 391-404.
18. S. I. Bae and S. Baik, "Sintering and grain growth of ultrapure alumina," *J. Mater. Sci.*, **28**, [15], 4197-204 (1993).
19. S. I. Bae and S. Baik, "Determination of critical concentrations of silica and/or calcia for abnormal grain growth in alumina," *J. Am. Ceram. Soc.*, **76**, [4], 1065-7 (1993).

20. I.-J. Bae and S. Baik, "Abnormal grain growth of alumina," *J. Am. Ceram. Soc.*, **80**, [5], 1149-56 (1997).
21. J. H. Yoo, J. C. Nam, and S. Baik, "Quantitative evaluation of glass-forming impurities in alumina: equivalent silica concentration (ESC)," *J. Am. Ceram. Soc.*, **82**, [8], 2233-8 (1999).
22. G. Wulff, "Zur Frage der Geschwindigkeit des Wachstums und der Auflösung der Krystallflachen," *Z. Krist.*, **34**, 449-530 (1901).
23. C. Herring, "Some Theorems on the Free Energy of Crystal Surfaces," *Phys. Rev.*, **82**, [1], 87-93 (1951).
24. J. Choi, D. Kim, B. J. Hockey, S. M. Wiederhorn, C. A. Handwerker, J. E. Blendell, W. C. Carter, and A. R. Roosen, "The Equilibrium Shape of Internal Cavities in Sapphire," *J. Am. Ceram. Soc.*, **80**, [1], 62-68 (1997).
25. M. Kitayama, "The Wulff Shape of Doped and Undoped Sapphire," Ph.D. thesis, Department of Materials Science and Mineral Engineering, University of California, Berkeley, (1996).
26. M. Kitayama and A. M. Glaeser, "The Energetics and Kinetics of Pore Shape Evolution in Alumina," *Key Eng. Mater.*, **159-160**, 193-204 (1999).
27. M. Kitayama, T. Narushima, and A. M. Glaeser, "The Wulff Shape of Alumina: II. Experimental Measurement of Pore Shape Evolution," *J. Am. Ceram. Soc.*, **83**, [10], 2572-2583 (2000).
28. M. Kitayama and A. M. Glaeser, "The Wulff Shape of Alumina: III. Undoped Alumina," *in preparation*.
29. M. Kitayama and A. M. Glaeser, "The Wulff Shape of Alumina: IV. Ti(IV)-Doped Alumina," *in preparation*.
30. M. Kitayama and A. M. Glaeser, "The Wulff Shape of Alumina: V. Mg, Ca, and Ti(III)-doped Alumina," *in preparation*.
31. C. Sung, G. C. Wei, K. J. Ostreicher, and W. H. Rhodes, "Segregation of magnesium to the internal surface of residual pores in translucent polycrystalline alumina," *J. Am. Ceram. Soc.*, **75**, [7], 1796-800 (1992).
32. D. W. Susnitzky and C. B. Carter, "Identification of alpha-alumina surface structures by electron diffraction," *J. Am. Ceram. Soc.*, **69**, [9], C217-20 (1986).
33. M. Gautier, J. P. Duraud, L. Pham Van, and M. J. Guitter, "Modifications of alpha-Al_2O_3(0001) surfaces induced by thermal treatments of ion bombardment," *Surf. Sci.*, **250**, [1-3], 71-80 (1991).
34. M. Gautier, G. Renaud, L. P. Van, B. Villette, M. Pollak, N. Thromat, F. Jollet, and J. P. Duraud, "α-Al_2O_3 (0001) surfaces: atomic and electronic structure," *J. Am. Ceram. Soc.*, **77**, [2], 323-34 (1994).
35. W. D. Kaplan, H. Mullejans, M. Ruhle, J. Rodel, and N. Claussen, "Ca segregation to basal surfaces in alpha-alumina," *J. Am. Ceram. Soc.*, **78**, [10], 2841-4 (1995).
36. H. P. Bonzel and W. W. Mullins, "Smoothing of perturbed vicinal surfaces," *Surf. Sci.*, **350**, [1], 285-300 (1996).
37. C. Duport, A. Chame, W. W. Mullins, and J. Villain, "Decay of Grooves Cut in a Surface with Singular Orientation when the Neighboring Orientations are Unstable," *J. Phys. I*, **6**, [8], 1095-1125 (1996).
38. W. W. Mullins and G. S. Rohrer, "Nucleation Barrier for Volume-Conserving Shape Changes of Faceted Crystals," *J. Am. Ceram. Soc.*, **83**, [1], 214-16 (2000).

39. M. Kitayama, J. D. Powers, L. Kulinsky, and A. M. Glaeser, "Surface and interface properties of alumina via model studies of microdesigned interfaces," *J. Eur. Ceram. Soc.*, **19**, [13-14], 2191-209 (1999).
40. M. Kitayama, T. Narushima, W. C. Carter, R. M. Cannon, and A. M. Glaeser, "The Wulff Shape of Alumina: I. Modelling the Kinetics of Morphological Evolution," *J. Am. Ceram. Soc.*, **83**, [10], 2561-2571 (2000).
41. J. Rödel and A. M. Glaeser, "High-Temperature Healing of Lithographically Introduced Cracks in Sapphire," *J. Am. Ceram. Soc.*, **73**, [3], 592-601 (1990).
42. J. Rödel and A. M. Glaeser, "Morphological Evolution of Pore Channels in Alumina," in Sintering of Advanced Ceramics, vol. 7, *Ceramic Transactions*, C. A. Handwerker, J. E. Blendell, and W. A. Kaysser, Eds. Westerville, OH: The American Ceramic Society, 1990, pp. 243-57.
43. J. D. Powers and A. M. Glaeser, "High-Temperature Healing of Cracklike Flaws in Mg- and Ca-Ion-Implanted Sapphire," *J. Am. Ceram. Soc.*, **75**, [9], 2547-58 (1992).
44. J. D. Powers and A. M. Glaeser, "High-Temperature Healing of Cracklike Flaws in Titanium Ion-Implanted Sapphire," *J. Am. Ceram. Soc.*, **76**, [9], 2225-34 (1993).
45. L. Kulinsky, J. D. Powers, and A. M. Glaeser, "Morphological Evolution of Pre-perturbed Pore Channels in Sapphire," *Acta Mater.*, **44**, [10], 4115-30 (1996).
46. J. D. Powers and A. M. Glaeser, "Orientation Effects on the High-Temperature Morphological Evolution of Pore Channels in Sapphire," *J. Am. Ceram. Soc.*, **83**, [9], 2297-2304 (2000).
47. M. T. Plateau, "On the recent theories of the constitution of jets of liquid issuing from circular orifices," *Philos. Mag. S4*, **12**, [79], 286-97 (1856).
48. L. Rayleigh, "On the Instability of Jets," *Proc. London Math. Soc.*, **10**, 4-13 (1879).
49. L. Rayleigh, as cited in Hydrodynamic and Hydromagnetic Stability. New York: Dover Publications, 1981.
50. F. A. Nichols and W. W. Mullins, "Morphological Changes of a Surface of Revolution due to Capillarity-Induced Surface Diffusion," *J. Appl. Phys.*, **36**, [6], 1826-35 (1965).
51. F. A. Nichols and W. W. Mullins, "Surface (Interface) and Volume-Diffusion Contributions to Morphological Changes Driven by Capillarity," *Trans. A.I.M.E.*, **233**, [10], 1840-48 (1965).
52. S. A. Hackney, "On the linear instability of the Rayleigh spheroidization process," *Scr. Metall. Mater.*, **25**, [4], 799-804 (1991).
53. Q. Ma, "A Model For the Breakup of Rod Morphologies," *Scr. Mater.*, **36**, [1], 77-82 (1997).
54. R. F. Sekerka and T. F. Marinis, "Dynamics of Morphological Change during Solid-Solid Transformations," in Solid → Solid Phase Transformations, H. I. Aaronson, D. E. Laughlin, R. F. Sekerka, and C. M. Wayman, Eds. New York: The Metallurgical Society of AIME, 1982, pp. 67-84.
55. Q. Ma, "Non-linear capillary shape evolution of rod morphologies via interfacial diffusion," *Acta Mater.*, **46**, [5], 1669-81 (1998).
56. J.-H. Choy, S. A. Hackney, and J. K. Lee, "Nonlinear stability analysis of the diffusional spheroidization of rods," *J. Appl. Phys.*, **77**, [11], 5647-54 (1995).
57. F. A. Nichols, "On the spheroidization of rod-shaped particles of finite length," *J. Mater. Sci.*, **11**, [6], 1077-82 (1976).
58. J. W. Cahn, "Stability of rods with anisotropic surface free energy," *Scr. Metall.*, **13**, [11], 1069-71 (1979).

59. J. S. Stölken and A. M. Glaeser, "The Morphological Evolution of Cylindrical Rods with Anisotropic Surface Free Energy via Surface Diffusion," *Scr. Metall. Mater.*, **27**, [4], 449-54 (1992).
60. A. M. Glaeser, "A New Approach to Investigating Surface Transport in Ceramics," in Mass and Charge Transport in Ceramics, vol. 71, *Ceramic Transactions*, K. Koumoto, L. M. Sheppard, and H. Matsubara, Eds. Westerville: The American Ceramic Society, 1996, pp. 117-36.
61. L. Crane, S. Birch, and P. D. McCormack, "The Effect of Mechanical Vibration on the Break-up of a Cylindrical Water Jet in Air," *Brit. J. Appl. Phys.*, **15**, [6], 743-50 (1964).
62. P. Vassallo and N. Ashgriz, "Satellite formation and merging in liquid jet breakup," *Proceedings of the Royal Society of London, Series A (Mathematical and Physical Sciences)*, **433**, [1888], 269-86 (1991).
63. O. Maruyama and W. Komatsu, "Observations on the grain-boundary of Al_2O_3 bicrystals," *Ceramurgia International*, **5**, [2], 51-5 (1979).
64. M. De Graef, B. J. Dalgleish, M. R. Turner, and A. G. Evans, "Interfaces between alumina and platinum: structure, bonding and fracture resistance," *Acta Metall. Mater.*, **40**, [Supplement], S333-44 (1992).
65. W. C. Carter and A. M. Glaeser, "The morphological stability of continuous intergranular phases: thermodynamic considerations," *Acta Metall.*, **35**, [1], 237-45 (1987).
66. F. P. Mallinder and B. A. Proctor, "Preparation of High-Strength Sapphire Crystals," *Proc. Brit. Ceram. Soc.*, **6**, [1], 9-16 (1966).
67. A. H. Heuer and J. P. Roberts, "The Influence of Annealing on the Strength of Corundum Crystals," *Proc. Brit. Ceram. Soc.*, **6**, [1], 17-27 (1966).
68. L. M. Davies, "The Effect of Heat Treatment on the Tensile Strength of Sapphire," *Proc. Brit. Ceram. Soc.*, **6**, [1], 29-35 (1966).
69. F. F. Lange and K. C. Radford, "Healing of surface cracks in polycrystalline Al_2O_3," *J. Am. Ceram. Soc.*, **53**, [7], 420-1 (1970).
70. B. J. Hockey and B. R. Lawn, "Electron microscopy of microcracking about indentations in aluminium oxide and silicon carbide," *J. Mater. Sci.*, **10**, [8], 1275-84 (1975).
71. T. K. Gupta, "Crack healing and strengthening of thermally shocked alumina," *J. Am. Ceram. Soc.*, **59**, [5-6], 259-62 (1976).
72. A. G. Evans and E. A. Charles, "Strength recovery by diffusive crack healing," *Acta Metall.*, **25**, [8], 919-27 (1977).
73. J. Rödel and A. M. Glaeser, "Microdesigned Interfaces: New Opportunities for Materials Science," *Yogyo Kyokai Shi*, **99**, [4], 251-65 (1991).
74. S. Surnev, B. Voigtlander, H. P. Bonzel, and W. W. Mullins, "Anisotropic profile decay on perturbed Au(111) vicinal surfaces," *Surf. Sci.*, **360**, [1-3], 242-8 (1996).
75. T. Narushima and A. M. Glaeser, "High-Temperature Morphological Evolution of Lithographically Introduced Cavities in Silicon Carbide," in review, *J. Am. Ceram. Soc.*.
76. H. P. Bonzel, E. Preuss, and B. Steffen, "Periodic Surface Profiles Under the Influence of Anisotropic Surface Energy: A Steady-State Solution," *Surf. Sci.*, **145**, [1], 20-32 (1984).
77. H. P. Bonzel, E. Preuss, and B. Steffen, "The Dynamical Behavior of Periodic Surface Profiles on Metals Under the Influence of Anisotropic Surface Energy," *J. Appl. Phys. A (Solids and Surfaces)*, **35**, [1], 1-8 (1984).
78. U. Breuer and H. P. Bonzel, "Morphology of Periodic Surface Profiles on Au Single Crystals and the Anisotropy of the Surface Free Energy of Au," *Surf. Sci.*, **273**, [1], 219-36 (1992).
79. E. Mammana, R. A. Marks, and A. M. Glaeser, *unpublished research* (1998).
80. A. M. Glaeser, "The morphological instability of a facetted rod," *unpublished research* (1997).

Tables

Table 1: Pore Channel Breakup in Ca-Implanted Sapphire [43]

	R = 0.32 μm	R = 0.50 μm	R = 0.71 μm
Minimum λ/R	19.4	22.2	19.0
Maximum λ/R	116	124	113
Data Points	192	247	224
Mean λ/R	62.8	64.6	61.7
Std Deviation (% of mean)	20.1 (32.0)	20.8 (32.2)	18.5 (30.0)

Table II Tabulation of λ_{max} for Undoped and Ti-doped Sapphire

Undoped (0001) Sapphire

Channel Orientation	λ_{max}/R	Notes	Reference
$[1\bar{1}00](0001)$	30.2-37.4	Unperturbed, low-angle twist (<2°)	[42]
$[11\bar{2}0](0001)$	>200		
$[1\bar{1}00](0001)$	70	Unperturbed, low-angle twist (<2°)	[46]
$[11\bar{2}0](0001)$	195		
$[1\bar{1}00](0001)$	45	Unperturbed, basal twin	[44]
$[11\bar{2}0](0001)$	130		
$[1\bar{1}00](0001)$	45	Unperturbed, basal twin	[46]
$[11\bar{2}0](0001)$	135		
$[1\bar{1}00](0001)$	24-30	Preperturbed, low-angle twist	[45]
$[11\bar{2}0](0001)$	42-56 48-60		
$[1\bar{1}00](0001)$	38-113	Preperturbed, 5° basal twist	*unpublished*
$[1\bar{1}00](0001)$	33-66	Preperturbed, <1° basal twist	*unpublished*
$[11\bar{2}0](0001)$	36-60	Preperturbed, 4° basal twist	*unpublished*

Ti-doped (0001) Sapphire

Channel Orientation	λ_{max}/R	Notes	Reference
$[1\bar{1}00](0001)$	∞	Unperturbed, basal twin, Ti-implanted	[44]
$[11\bar{2}0](0001)$	78		
$[1\bar{1}00](0001)$	not defined	Preperturbed, low-angle twist melt-grown Ti-doped sapphire	*unpublished*
$[11\bar{2}0](0001)$	22-33		
$[1\bar{1}00](0001)$	17-23	Preperturbed, <1° twist melt-grown Ti-doped sapphire	*unpublished*

Figure Captions:

Figure 1 Schematic illustration of the morphological evolution associated with Rayleigh instabilities. In (a), a segment of an infinitely long cylinder is shown. Infinitesimal perturbations in the radius either shrink (decay) or grow with time. In (b)-(d), the progressive increase in perturbation amplitude is shown. In the idealized situation illustrated, the wavelength that controls the ultimate particle or pore spacings is the kinetically dominant wavelength, λ_{max}.

Figure 2 Optical micrograph of a) 10 μm wide by ≈0.15 micron deep pore channels at an internal interface after bonding but prior to any annealing. During the initial stages of annealing a more equiaxed cross sectional shape develops. Subsequently, perturbations develop along the pore channel axis, as illustrated in (b). At a later stage of evolution (c), isolated pores form due to the continued increase in perturbation amplitude. Note the variation in pore spacings.

Figure 3 Optical micrographs of pore channel arrays used to assess the effects of orientation and aspect ratio on pore channel evolution. In (a), high aspect ratio pore channels of ≈3 μm width are arranged in a spoke pattern, with the channels rotated in 15° increments over the full 360° range. In (b), each "spoke" contains an array of individual channels of controlled and progressively increasing aspect ratio.

Figure 4 Normalized pore spacing distributions following the breakup of pore channels oriented parallel to $[11\bar{2}0]$ in calcium-implanted sapphire wafers. Samples were annealed at 1700°C.

Figure 5 Example of pore channels with imposed perturbations of controlled wavelength and fixed amplitude. In (a), the pore channel geometry after bonding but before annealing is illustrated in an optical micrograph. The perturbation wavelengths increase from top to bottom, and are 25, 37.5, 50, 62.5, and 75 μm. Each channel is 7500 μm long. Five additional channels that span the wavelength range from 100 to 250 μm are included in the pattern, but are not shown. In (b), sections of the channels in (a) are shown after 10 h of annealing at 1650°C, and prior to breakup. Note the lateral contraction that has occurred due to the development of a more nearly equiaxed cross section. In (c) and (d), channels with wavelengths of 100, 125, 150, 200 and 250 μm are shown after 90 h at 1650°C. The channels are largely broken up with pore spacings reflecting the imposed wavelength, although in some cases smaller "satellite" pores also form (*see second channel from bottom*). Note that not all regions of every channel evolve identically. The shorter wavelength channels were either not broken up, or exhibited less uniform breakup behavior with pore spacings differing from λ_{imp}.

Figure Captions: (cont.)

Figure 6 Optical micrographs of preperturbed pore channels oriented along $[1\bar{1}00]$. In (a), a pattern with λ_{imp}=25 μm, shows breakup prior to cross-sectional equilibration. Note that the apparent width of the residual pores is ≈30 μm, the mean width of the etched in features, and the lack of periodicity. In (b), longer wavelength (200 μm) channels of the same orientation in the same sample showed the development of unperturbed edges. Since the perturbation amplitude is fixed, the misorientation range sampled by the bounding surface increases as λ_{imp} decreases. In a second sample, (c) channels with λ_{imp}=25 μm and nominally identical orientation did not break up within 35 h at 1650°C, but edge regression is evident. Channels with λ_{imp} = 37.5 μm, (d), did break up in a more "normal" manner.

Figure 7 Subsets of the mask pattern illustrated in Figure 3b, introduced into undoped sapphire, after annealing for 12 h at 1700°C. As the aspect ratio increases within each set, the transition from one to two to in some cases three or four particles is observed. The critical aspect ratios for these transitions and the evolution rate depend upon the crystallographic orientation of the channels that make up each array. The directions indicated as **e** and **g** are $[11\bar{2}0]$ and $[1\bar{1}00]$, respectively.

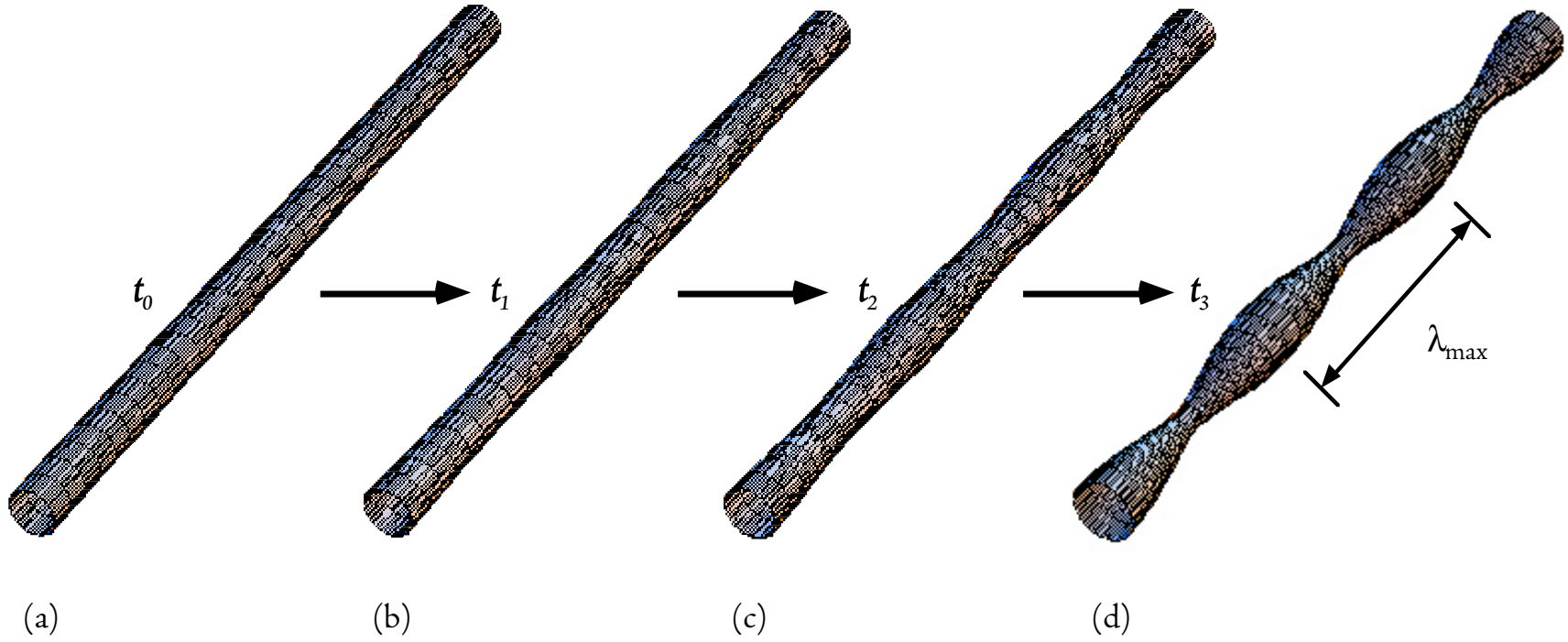

Figure 1 Schematic illustration of the morphological evolution associated with Rayleigh instabilities. In (a), a segment of an infinitely long cylinder is shown. Infinitesimal perturbations in the radius either shrink (decay) or grow with time. In (b)-(d), the progressive increase in perturbation amplitude is shown. In the idealized situation illustrated, the wavelength that controls the ultimate particle or pore spacings is the kinetically dominant wavelength, λ_{max}.

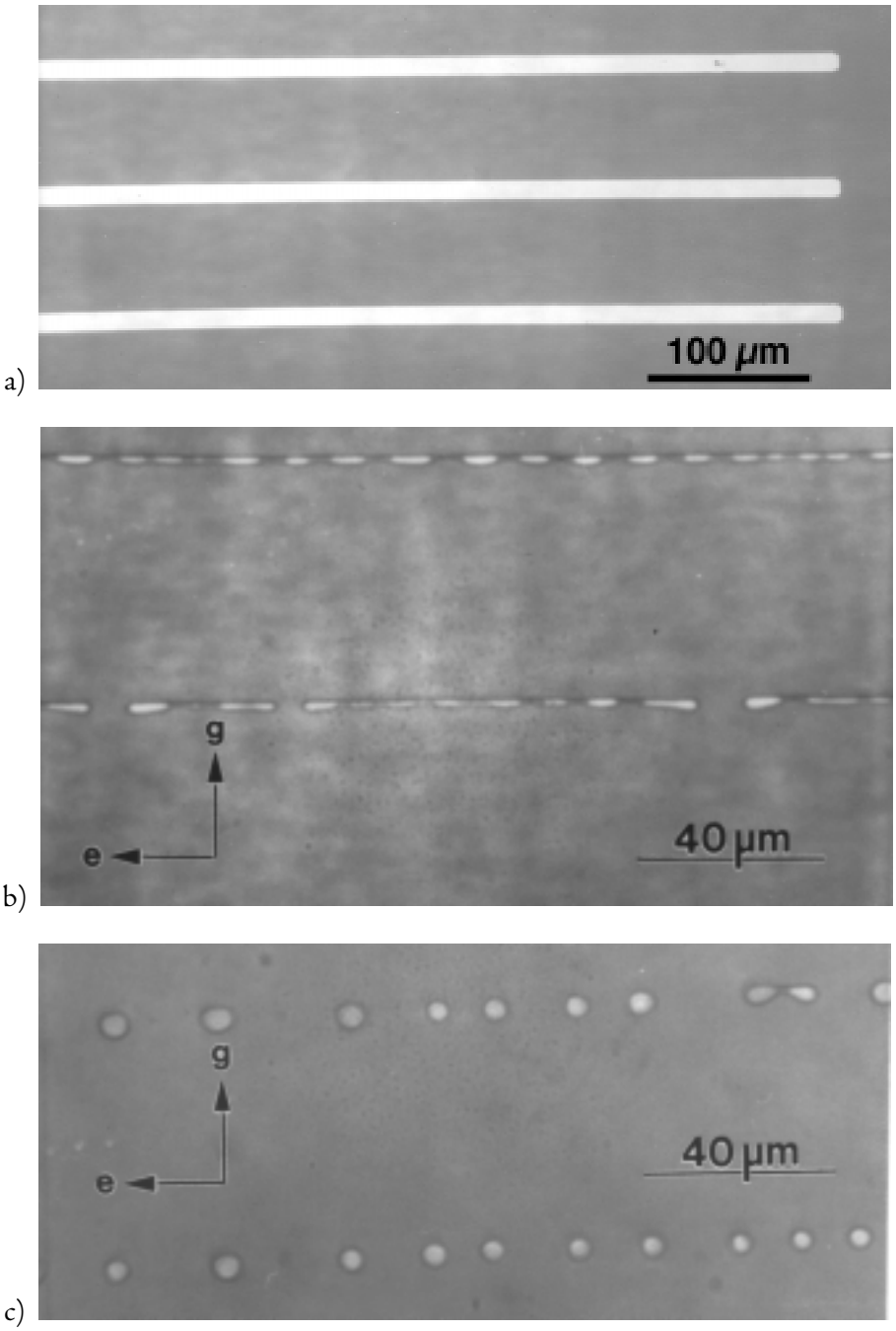

Figure 2 Optical micrograph of a) 10 μm wide by ≈0.15 micron deep pore channels at an internal interface after bonding but prior to any annealing. During the initial stages of annealing a more equiaxed cross sectional shape develops. Subsequently, perturbations develop along the pore channel axis, as illustrated in (b). At a later stage of evolution (c), isolated pores form due to the continued increase in perturbation amplitude. Note the variation in pore spacings.

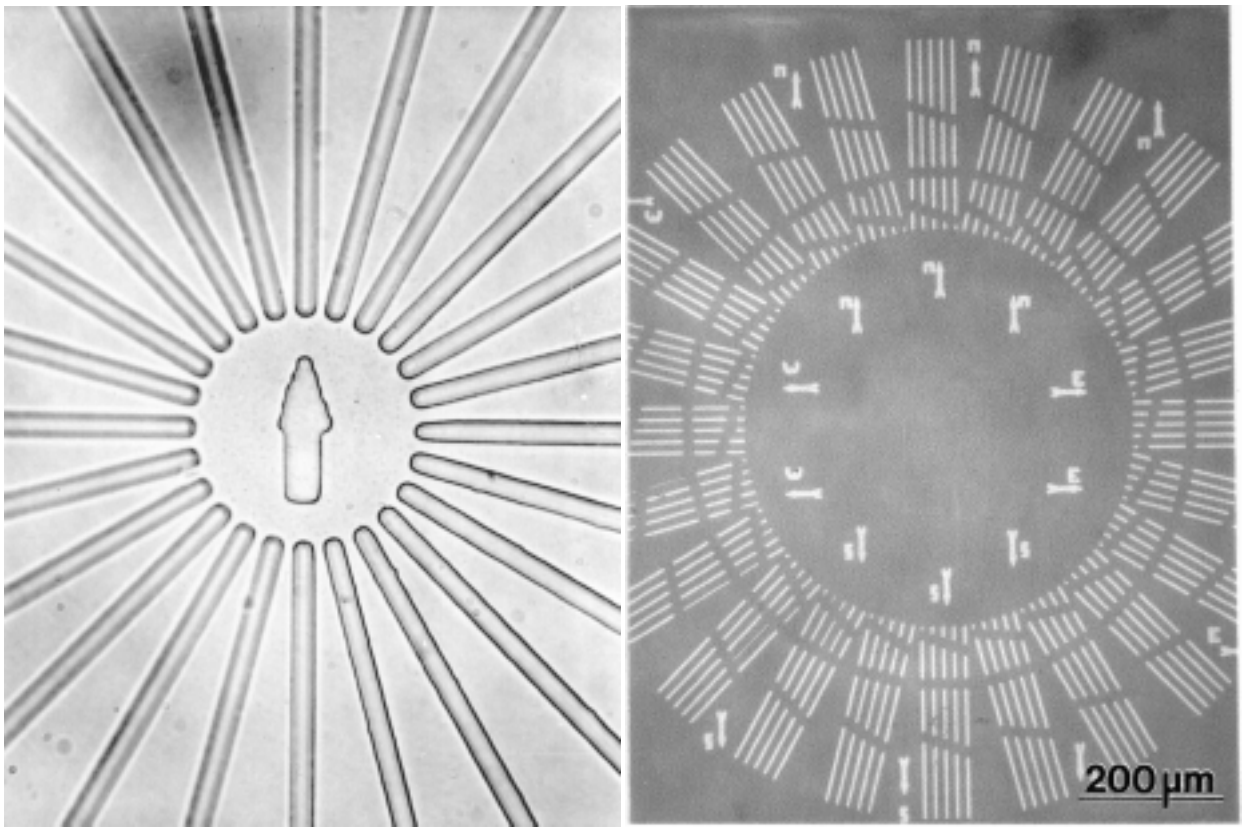

(a) (b)

Figure 3 Optical micrographs of pore channel arrays used to assess the effects of orientation and aspect ratio on pore channel evolution. In (a), high aspect ratio pore channels of ≈3 µm width are arranged in a spoke pattern, with the channels rotated in 15° increments over the full 360° range. In (b), each "spoke" contains an array of individual channels of controlled and progressively increasing aspect ratio.

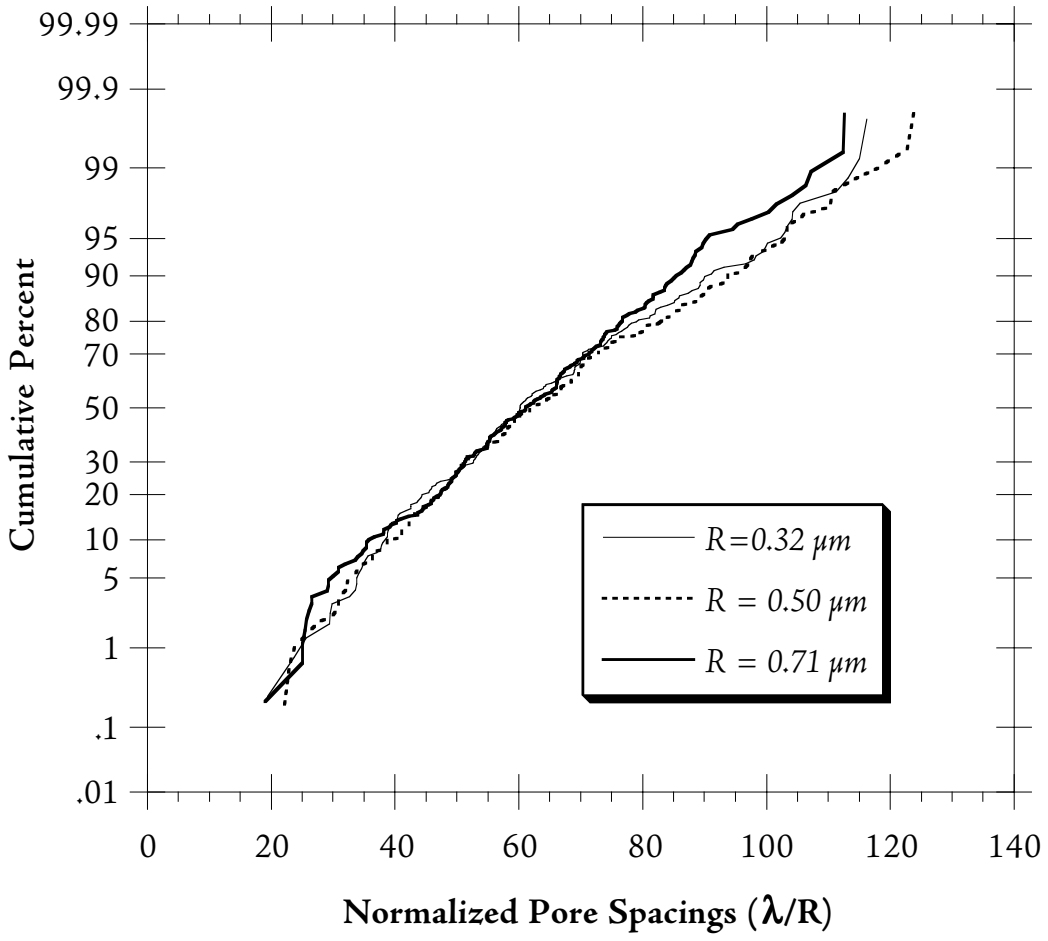

Figure 4 Normalized pore spacing distributions describing the breakup characteristics of pore channels oriented parallel to [11$\bar{2}$0] in calcium-implanted sapphire wafers. Samples were annealed at 1700°C.

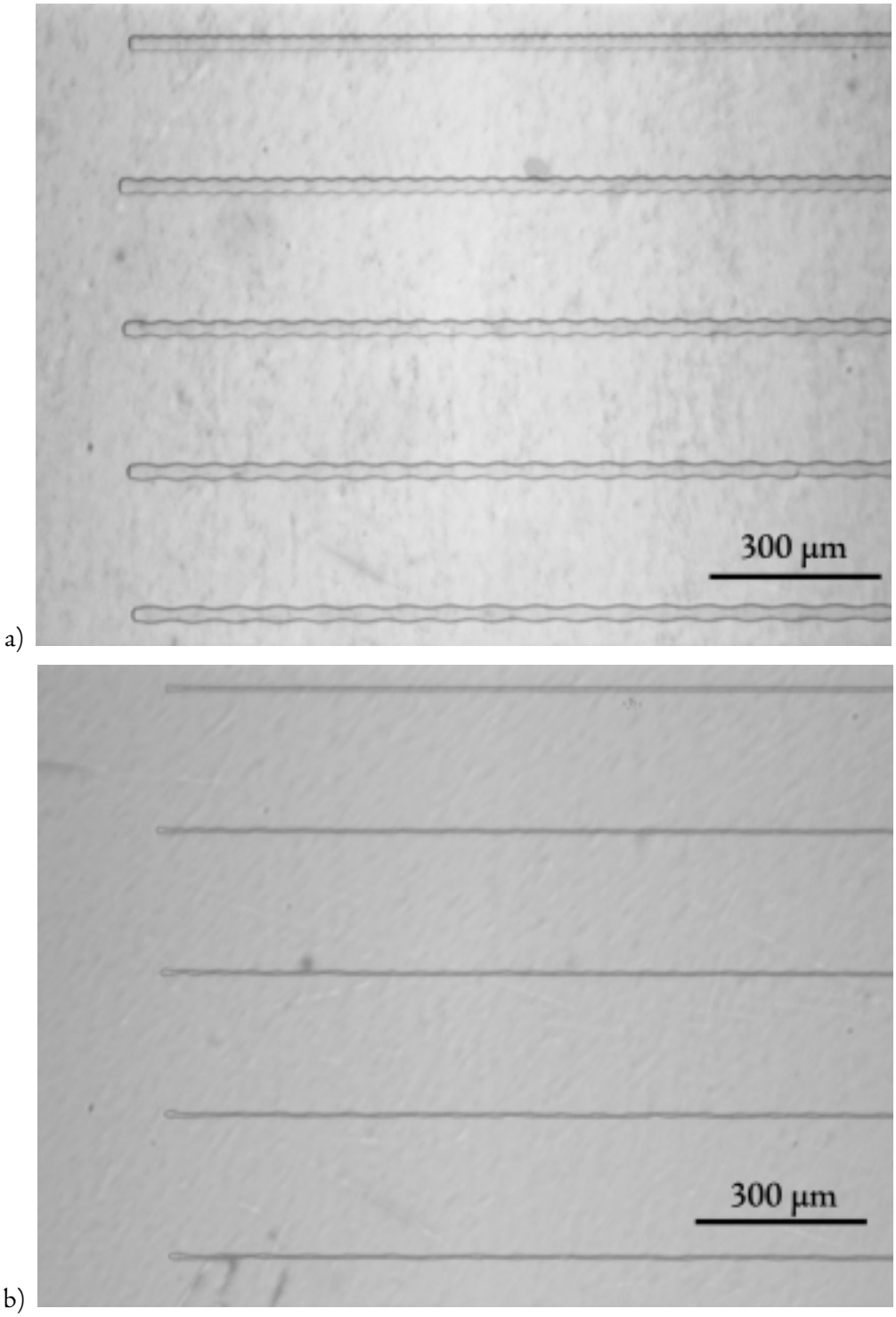

Figure 5 Example of pore channels with imposed perturbations of controlled wavelength and fixed amplitude. In (a), the pore channel geometry after bonding but before annealing is illustrated in an optical micrograph. The perturbation wavelengths increase from top to bottom, and are 25, 37.5, 50, 62.5, and 75 μm. Each channel is 7500 μm long. Five additional channels that span the wavelength range from 100 to 250 μm are included in the pattern, but are not shown. In (b), sections of the channels in (a) are shown after 10 h of annealing at 1650°C, and prior to breakup. Note the lateral contraction that has occurred due to the development of a more nearly equiaxed cross section.

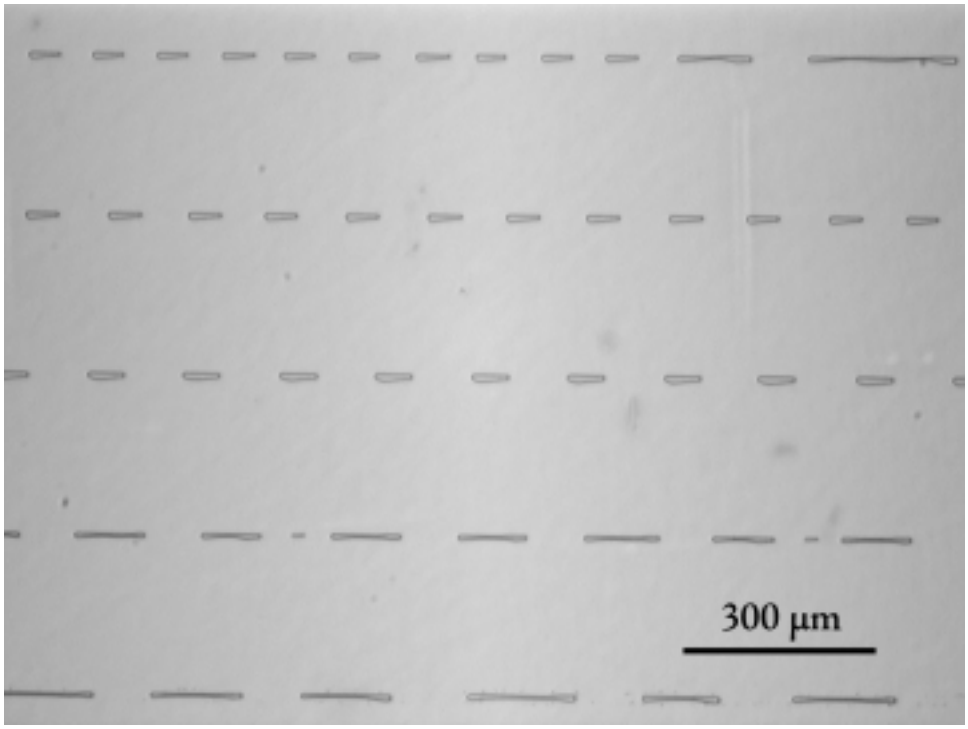

c)

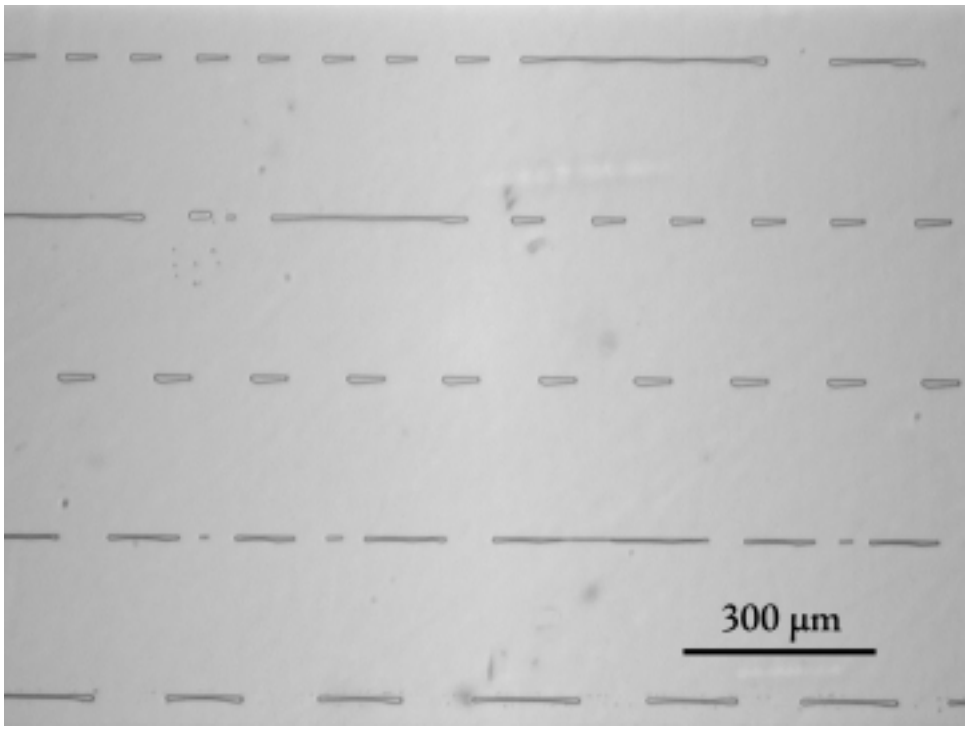

d)

Figure 5 In (c) and (d), channels with wavelengths of 100, 125, 150, 200 and 250 µm are shown after 90 h at 1650°C. The channels are largely broken up with pore spacings reflecting the imposed wavelength, although in some cases smaller "satellite" pores also form (*see second channel from bottom*). Note that not all regions of every channel evolve identically. The shorter wavelength channels were either not broken up, or exhibited less uniform breakup behavior with pore spacings differing from λ_{imp}.

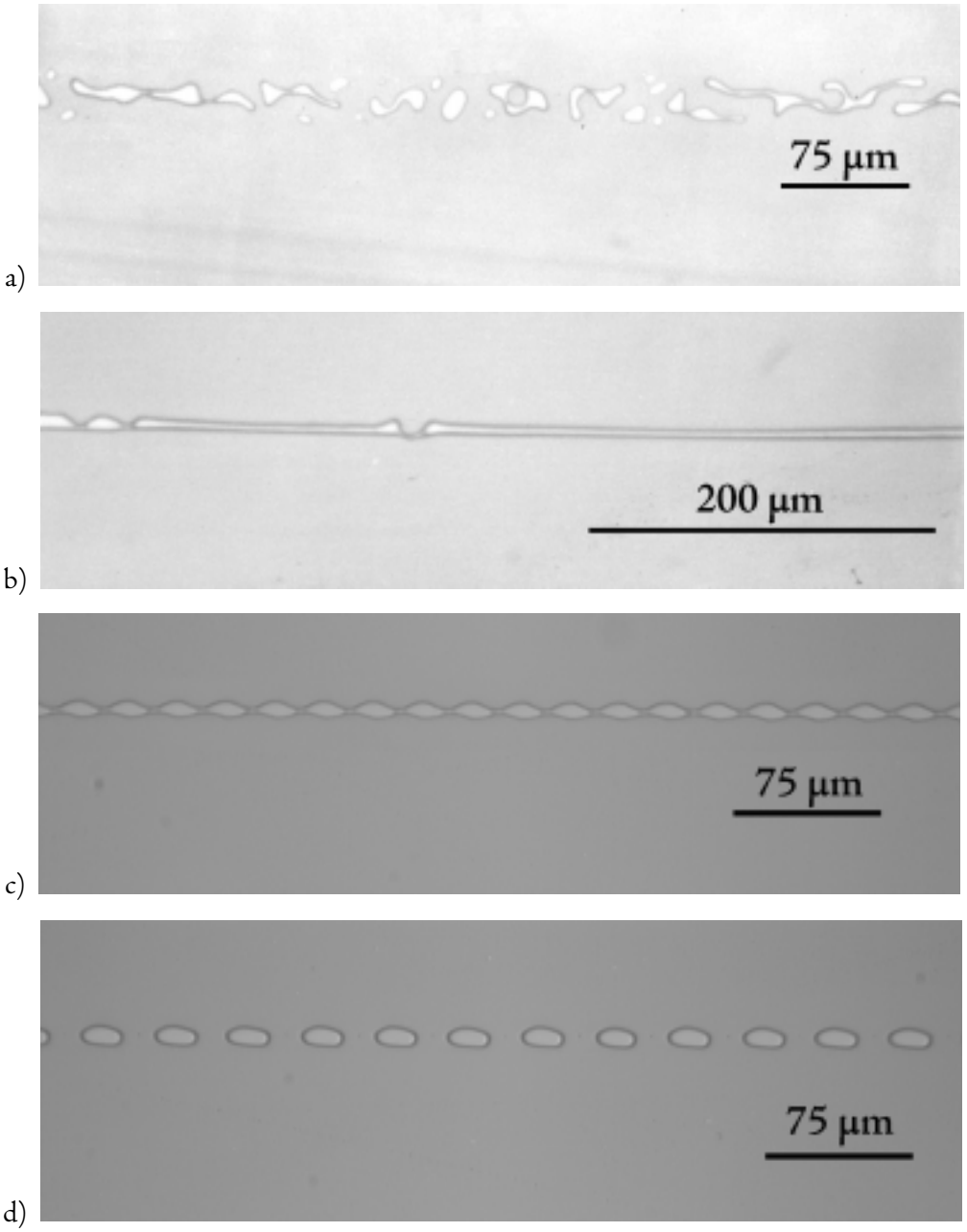

Figure 6 Optical micrographs of preperturbed pore channels oriented along $[1\bar{1}00]$. In (a), a pattern with λ_{imp}=25 μm, shows breakup prior to cross-sectional equilibration. Note that the apparent width of the residual pores is ≈30 μm, the mean width of the etched in features, and the lack of periodicity. In (b), longer wavelength (200 μm) channels of the same orientation in the same sample showed the development of unperturbed edges. Since the perturbation amplitude is fixed, the misorientation range sampled by the bounding surface increases as λ_{imp} decreases. In a second sample, (c) channels with λ_{imp}=25 μm and nominally identical orientation did not break up within 35 h at 1650°C, but edge regression is evident. Channels with λ_{imp} = 37.5 μm, (d), did break up in a more "normal" manner.

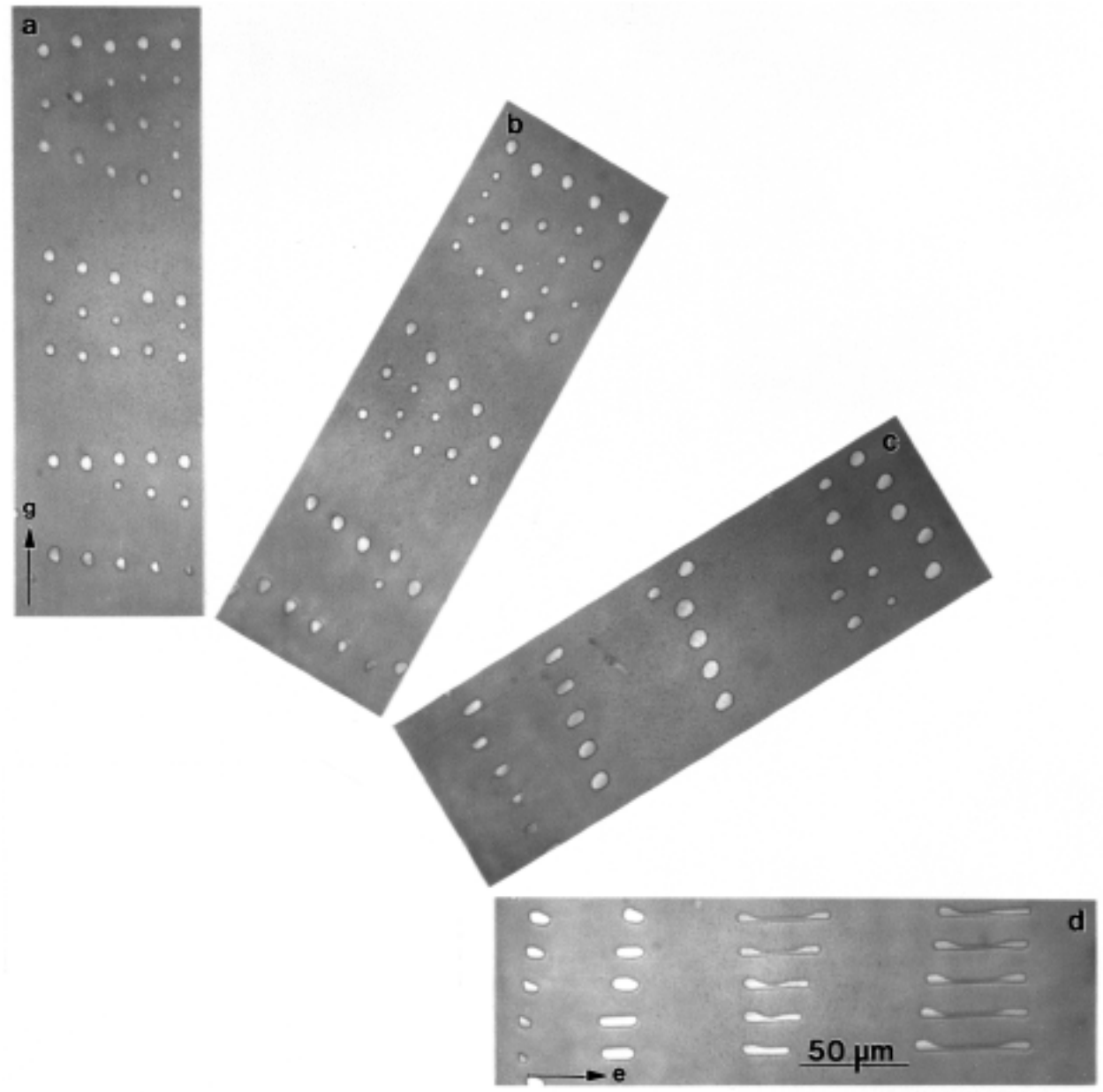

Figure 7 Subsets of the mask pattern illustrated in Figure 3b, introduced into undoped sapphire, after annealing for 12 h at 1700°C. As the aspect ratio increases within each set, the transition from one to two to in some cases three or four particles is observed. The critical aspect ratios for these transitions and the evolution rate depend upon the crystallographic orientation of the channels that make up each array. The directions indicated as **e** and **g** are $[11\bar{2}0]$ and $[1\bar{1}00]$, respectively.